FEUP FACULDADE DE ENGENHARIA
UNIVERSIDADE DO PORTO

Departamento de Engenharia Química

Polymeric micro- and nanoparticles for delivery of therapeutic peptides

Luís Carlos Pinto dos Santos Pissarra Moutinho

Licenciado em Ciências Farmacêuticas pela

Faculdade de Farmácia da Universidade do Porto

Dissertação submetida para satisfação dos requisitos do

grau de mestre em Engenharia Biomédica

Dissertação realizada sob a supervisão da Professora Doutora Maria do Carmo Pereira (orientadora) e da Doutora Sandra Rocha (co-orientadora), do Departamento de Engenharia Química da Faculdade de Engenharia da Universidade do Porto

Porto, Fevereiro de 2010

Resumo

Esta tese apresenta dois nano-sistemas poliméricos, designadamente poli(L-lisina)/ácido poli(L-glutâmico), e quitosano/goma arábica, como potenciais veículos de administração de moléculas terapêuticas como o péptido iAβ5. Este pentapéptido é capaz de inibir, *in vitro*, as alterações conformacionais do péptido β-amilóide que levam à formação de placas de amilóide na doença de Alzheimer. No entanto, sequências com poucos aminoácidos apresentam normalmente reduzida biodisponibilidade e baixo tempo de semi-vida plasmático.

Nanopartículas e nanocápsulas de poli(L-lisina) (PLL)/ácido poli(L-glutâmico) (PLG) foram produzidas pela técnica de adsorção sequencial dos polímeros. O iAβ5 foi incorporado entre as camadas poliméricas das nanopartículas e encapsulado nas nanocápsulas por alteração de pH. A incorporação do iAβ5 entre as camadas das nanopartículas demonstrou ser um processo mais eficiente para proteger o péptido do que a encapsulação. A interacção *in vitro* dos nano-sistemas PLL/PLG com células de neuroblastoma foi estudada, usando a linha celular SH-SY5Y. A internalização celular das nanopartículas foi observada sem alteração da morfologia celular original.

Nanopartículas esféricas de quitosano (CS)/goma arábica (GA), a várias proporções de cargas CS:GA, foram produzidas por complexação polielectrolítica. O diâmetro hidrodinâmico e o potencial zeta das nanopartículas não variaram significativamente com o aumento do número de cargas negativas (goma arábica). Os valores positivos de potencial zeta explicam-se pelas cargas positivas livres (não neutralizadas) estabilizadas à superfície. A formação de estruturas vesiculares foi observada a baixa concentração global de biopolímeros e parece resultar de uma insuficiente neutralização das cargas.

Abstract

This thesis presents two polymeric systems, namely poly(L-lysine)/poly(L-glutamic acid) nanoparticles and nanocapsules, and chitosan/gum arabic nanoparticles, potentially suitable for the delivery of therapeutic molecules such as the iAβ5 peptide. The iAβ5 is a pentapeptide capable of *in vitro* inhibition of the conformational changes of amyloid-β peptide which lead to amyloid plaque formation in Alzheimer's disease. However, short peptides have a low bioavailability and a short half-life in the bloodstream.

Poly(L-lysine) (PLL)/poly(L-glutamic acid) (PLG) nanoparticles and nanocapsules were produced by the layer-by-layer technique. The iAβ5 peptide was entrapped within the polymeric layers of the nanoparticles and encapsulated in the nanocapsules by changing the pH. It has been shown that the entrapment of iAβ5 within the nanoparticle layers is a more efficient process for protecting the peptide, than the encapsulation in nanocapsules. The *in vitro* interaction of PLL/PLG nanosystems with neuroblastoma cells was carried out using the SH-SY5Y cell line. The cellular internalization of nanoparticles was achieved without altering the original cellular morphology.

Spherical chitosan (CS)/gum arabic (GA) nanoparticles were produced, at several CS:GA charge ratios, by polyelectrolyte complexation. The hydrodynamic diameter and zeta potential of the nanoparticles did not vary significantly with increasing the number of negative charges (gum arabic). The positive zeta potential values of the nanoparticles are explained by free, non-neutralized positive charges stabilized at the particle surface. The formation of vesicular structures was observed at low overall biopolymer concentration and might be a result of insufficient charge neutralization.

Acknowledgements

I would like to thank Prof. Maria do Carmo Pereira and Prof. Manuel Coelho for accepting me as MSc student in their laboratory at the Faculty of Engineering of the University of Porto.

I am very thankful to Prof. Maria do Carmo Pereira and Dr. Sandra Rocha, respectively my supervisor and co-supervisor, for their support and priceless comments, suggestions and corrections.

My gratitude extends to the rest of the members of my research group, for their ready help in the laboratory's tasks.

The several images and micrographs were obtained and interpreted with the valuable help of Paula Sampaio, from IBMC (CLSM images); Rui Fernandes, from IBMC (TEM micrographs); Rui Rocha from CEMUP and Anne Heilig from the Max Planck Institute of Colloids and Interfaces (AFM micrographs).

I would also like to thank Isabel Cardoso, from IBMC, for her help and support in the *in vitro* studies with SH-SY5Y cells.

This research was supported by the FCT research project PTDC/BIO/69359/2006.

Preface

Peptidic molecules show promising therapeutic responses. Although, their efficacy faces several limitations, including short half-life in the bloodstream and low bioavailability. It is known that nanoparticulate systems can improve the efficacy and/or reduce the toxicity of drugs by modifying their distribution, thus, the study and characterization of new nanocarriers is nowadays an endeavouring field of research.

This thesis focuses on the study of two polymeric systems, namely poly(L-lysine) (PLL)/poly(L-glutamic acid) (PLG) nanoparticles and nanocapsules, and chitosan (CS)/gum arabic (GA) nanoparticles, as potential vehicles for the delivery of therapeutic peptides. The State of the art (chapter 1) describes different types of nanocarriers that can be used as drug delivery systems, making reference to several materials and techniques employed in their production, and is followed by the description of the Methods used throughout the work (chapter 2).

Chapter 3 is dedicated to the PLL/PLG system. Nanoparticles and nanocapsules of the polypeptides were produced by the layer-by-layer self assembly technique. The beta-sheet breaker peptide iAβ5 was successfully entrapped within the polymeric layers of nanoparticles. The integrity of their polymeric walls was found to be resistant to acidic and alkaline pH values. In what concerns to nanocapsules, the integrity of their polymeric walls was also kept, along with their spherical shape and original diameter, after core removal. The encapsulation of the peptide was also achieved by permeability changes (pH shifting), although the entrapment within polymeric layers was able to retain the molecule more efficiently. *In vitro* internalization of PLL/PLG nanocapsules in neuroblastoma cells (SH-SY5Y cell line), without causing alteration of the original cellular morphology, was demonstrated.

The CS/GA system is described in chapter 4. Nanoparticles were produced by polyelectrolyte complexation. Turbidity measurements showed that the production of higher amounts of CS/GA nanoparticles was favoured both by higher numbers of negative charges (GA) added to the CS starting solutions and by higher concentrations of the polymeric solutions. Visible aggregation was obtained when the positive charges of CS were completely compensated by the negative charges of GA. The hydrodynamic diameter and the positive zeta potential of the nanoparticles were found not to significantly vary as a function of both the concentration of the CS starting solutions and the number of negative charges added.

The Conclusions, presented in chapter 5, finalize the thesis.

Contents

Figure Index

1 State of the art

It is known that recent years' advances in the field of nanotechnology have been extremely helpful in the achievement of pharmacology's goals, such as the protection of drugs from premature degradation after administration and the protection of healthy tissues from grave side effects of certain drugs (Couvreur and Vauthier, 2006). As an illustrative example, nucleic acids are a type of drugs whose therapeutic effect is completely dependent on their association with carriers (Alonso, 2004). Peptides and proteins are another example of therapeutic molecules whose health benefits will considerably improve by using delivery systems. These molecules are typically vulnerable to proteolytic and hydrolytic enzymes, resulting in short biological half-life in the blood stream (Li *et al.*, 2001).

There is a large number of different types of nanocarriers used as drug-delivery systems. They can be either lipidic (liposomes, solid lipid nanoparticles) or polymeric (polymer micelles, nanoparticles, nanocapsules), and their diameters can range from 10 nm to 1 μm (Couvreur and Vauthier, 2006). For the scope of this thesis, only the concept of nanoparticles will be approached. It includes nanospheres and nanocapsules.

Nanospheres are matrices where active molecules can be dissolved, entrapped or adsorbed, while nanocapsules are hollow spherical structures with a polymeric shell, and the active molecules can be either encapsulated in their interior or adsorbed to the shell (Reis *et al.*, 2006b). Mechanical or chemical means can be used for the production of nanoparticles, using natural, semi-synthetic or synthetic polymers (Reis *et al.*, 2006b).

Polyelectrolyte multilayers have been proposed for the production of nanoparticulate delivery systems with tunable composition, structure and surface properties

(Sukhorukov *et al.*, 2005), by varying the number of added layers, the pH of assembly, or the salt concentration (Johnston *et al.*, 2006; Sukhorukov *et al.*, 2005). The technique applied to the preparation of multilayers, known as layer-by-layer technique (LbL), was introduced by Decher (Decher, 1997) and is based on the consecutive deposition of oppositely charged polymers onto colloidal particles. Acting as templates, the colloidal particles may be removed at the end of the process, by means of dissolution using appropriate solvents and allowing the incorporation of bioactive molecules in the resulting hollow core (Ariga *et al.*, 2007; Caruso, 2004). Depending predominantly on electrostatic interactions, the technique can be applied to charged synthetic or natural polymers and oligomers, proteins and organic or inorganic colloidal templates (Johnston *et al.*, 2006; Sukhorukov *et al.*, 2005). The most frequently used and well characterized polyelectrolytic pair in the production of LbL microcapsules is the one composed by poly(sodium 4-styrene sulfonate) (PSS), a strong polyanionic polymer, and poly(allylamine hydrochloride) (PAH), a weak cationic polymer (Sukhorukov *et al.*, 2005). The reversible permeation of the shell of PAH/PSS nanocapsules is possible by varying the pH of the medium to acidic (<6) and alkaline (>8) values (Antipov *et al.*, 2002). The pH shifts are responsible for the creation of pores in the polyelectrolyte walls, at acidic values, allowing the encapsulation of molecules and the resealing of the pores, at alkaline values, preventing the release of the molecules (Sukhorukov *et al.*, 2005). The microcapsule permeability can also be tuned by using solvents such as acetone and ethanol, or by varying the salt concentration (Ibarz *et al.*, 2001). In addition, irreversible, temperature-dependent permeation can be achieved by incorporating thermosensitive co-polymers (Glinel *et al.*, 2003). Tuning the stability of polyelectrolyte nanocapsules has also been possible by using polypeptides with incorporated cysteine, an amino acid capable of crosslink. The crosslinked nanocapsules

were more stable. Alternatively, it is possible to make nanocapsules more resistant to proteolytic degradation, hence more stable, by using polypeptides that are capable of resisting to certain proteases (Haynie *et al.*, 2005).

If the colloidal template is not removed after the deposition of charged polymers, the obtained nanocarriers are equivalent to nanospheres, and in this case the active molecules can be entrapped within the polymeric layers. Nanospheres (and nanoparticles in a broader sense) can be prepared by different methods such as solvent evaporation, coacervation or *in situ* polymerization and using a variety of polymers such as poly(alkylcyanoacrylates), poly(lactic acid) or chitosan (Soppimath *et al.*, 2001). Being molecules of natural origin (Sinha and Kumria, 2001), polysaccharides are non-toxic, hydrophilic and biodegradable (Liu *et al.*, 2008). They frequently have hydrophilic groups such as hydroxyl and carboxyl, which can interact non-covalently with epithelia and mucous membranes, facilitating bioadhesion (Lee *et al.*, 2000). Several polysaccharides possess the advantageous properties mentioned above, such as chitosan (Agnihotri *et al.*, 2004), alginate (Sarmento *et al.*, 2006), and dextran sulfate (Chen *et al.*, 2007).

Chitosan is the cationic polysaccharide most frequently used in the preparation of nanoparticles. It has been covalently crosslinked by glutaraldehyde for the adsorption of a diuretic drug, furosemide (Zhi *et al.*, 2005). However, as glutaraldehyde is not biocompatible, other crosslinkers, such as succinic acid and tartaric acid, have been proposed (Bodnar *et al.*, 2005). Since ionic crosslinking is more favourable than covalent crosslinking, as it is performed under milder conditions and uses simpler procedures (Liu *et al.*, 2008), chitosan has been ionically crosslinked with pentasodium tripolyphosphate (TPP) (Calvo *et al.*, 1997). The negatively charged ions of this non-toxic crosslinker interact with the positively charged amino groups of chitosan (Jain and

Banerjee, 2008). Chitosan-TPP nanoparticles have been used to deliver molecules such as mitoxantrone, a drug used in breast cancer cells and its metastases (Lu *et al.*, 2006) and tetanus toxoid vaccine (Vila *et al.*, 2004). Intermolecular electrostatic interactions are another type of linkages that can be established between chitosan and other polyelectrolytes, such as glucomannan (Alonso-Sande *et al.*, 2006), carboxymethyl cellulose (Cui and Mumper, 2001) and poly(L-glutamic acid) (Dai *et al.*, 2007). The wide use of chitosan in the nanocarrier production field relies on the fact that chitosan nanoparticles are generally capable of incorporating bioactive compounds (de Campos *et al.*, 2004), as well as associating with proteins (Pan *et al.*, 2002), peptides, oligonucleotides and plasmids (Aktas *et al.*, 2005). They also promote the absorption of molecules through mucous surfaces (Illum, 1998; Pan *et al.*, 2002), as a result of the combination of their bioadhesive/mucoadhesive properties (Illum, 1998) and their capacity to transiently open the tight junctions between epithelial cells (Illum, 1998; Pan *et al.*, 2002). However, chitosan nanoparticles have some drawbacks, particularly when obtained by ionic crosslinking with TPP. For example, their positive surface charge can confer them slightly cytotoxicity (Chen *et al.*, 2007), and their stability and resistance to mechanical strength is lower when compared to chitosan nanoparticles prepared with dextran sulfate (Agnihotri *et al.*, 2004; Chen *et al.*, 2007).

The role of peptides and proteins as available therapeutic drugs is becoming gradually more significant, as their synthesis is becoming more feasible and the assessment of their physiopathological role is improving (Reis *et al.*, 2006b). Taking into account the limitations and specific characteristics of these molecules, it would be extremely advantageous to find delivery systems possessing a subcellular size, biocompatibility with cells and tissues, and being capable of crossing biological barriers (the blood brain barrier being the most challenging among them) and potentially displaying sustained-

release properties. For example, peptides with therapeutical action in the brain, as dalargin, a pentapeptide that acts as an anaesthetic agent, have been included in nanoparticulate systems (Teixidó and Giralt, 2008). Moreover, peptide-based drugs for the treatment and diagnosis of diseases of the central nervous system (CNS), such as Parkinson's disease (Amer *et al.*, 2006), and Alzheimer's disease (Kokkoni *et al.*, 2006), are attracting more attention. In fact, the inhibition and/or reversal of the conformational changes that lead to the formation of the pathological protein conformers and their progressive aggregation are a valuable approach to the treatment of Protein Misfolding Disorders (PMD), such as Alzheimer's disease (Estrada and Soto, 2006). The most frequent pathological features of Alzheimer's disease are amyloid plaques, which are mainly composed of an aggregated peptide, the amyloid-β (Aβ). It is known that the region of Aβ responsible for the recognition between Aβ molecules, which in turn will aggregate, spans the 16-20 residues. This KLVFF pentapeptidic hydrophobic domain is involved in the misfolding and aggregation of Aβ molecules (Estrada and Soto, 2006). Among various potential candidates for inhibiting Aβ aggregation, iAβ5, a peptide with five residues, was found to be efficient (Adessi and Soto, 2002; Soto *et al.*, 1996) in *in vitro*, cellular and animal models (Adessi and Soto, 2002). Its sequence is based on the central hydrophobic region within the N-terminal domain of Aβ, spanning aminoacids 17 to 21, *i. e.* leucine, valine, phenylalanine, phenylalanine and alanine, respectively (Adessi and Soto, 2002). Valine at position 18 was replaced by a proline residue (Estrada and Soto, 2006), given the fact that valine stabilizes the β-sheet conformation of the peptide, while proline cannot adopt that conformation (Wood *et al.*, 1995).

Crossing the Blood-Brain Barrier (BBB) is one of the most critical aspects for treating diseases that affect the CNS, such as Alzheimer's disease (Estrada and Soto, 2006).

BBB is a high-density network of non-fenestrated capillaries that surrounds both the brain and the spinal cord. The endothelial cells present on the BBB capillaries have tight junctions between them (Partridge, 1998). Thus, the BBB acts like an active filter, regulating the passage of substances between the blood and the brain (Calabria and Shusta, 2006). Hydrophilic drugs are not capable of crossing the BBB (Aktas *et al.*, 2005), making its overcoming an endeavour in what concerns to the administration of drugs such as neuropeptides (Vauthier *et al.*, 2003) and hydrophilic anticancer agents (Reis *et al.*, 2006b). The use of peptides and proteins as therapeutic agents has got an additional drawback, besides the low bioavailability that results from their difficulty to cross the BBB: they have also a short half-life in the bloodstream, once absorbed (Reis *et al.*, 2006b). Thus, the linking of these molecules with nanoparticles could surpass these limitations and significantly improve their therapeutic efficacy.

2 Methods

2.1 Atomic Force Microscopy

Atomic force microscopy is a microscopy technique which enables the evaluation of the properties of surfaces at the atomic level, being very useful to study surfaces of biological materials and nanoscale structures. AFM can determine roughness, adhesion force, and nanometer sized dimensions of materials. Briefly, the operating mode is as follows (figure 2.1).

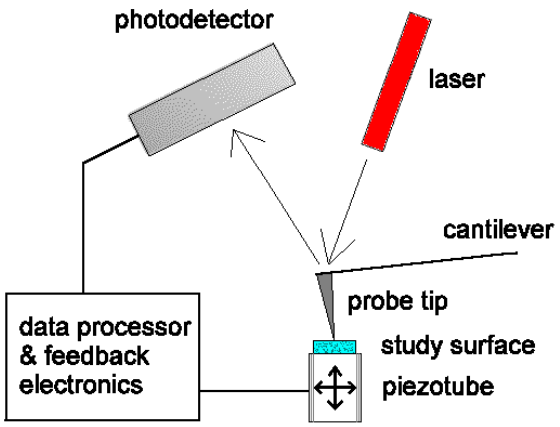

Figure 2.1 - The components of an atomic force microscope (retrieved from http://www.mobot.org/jwcross/spm/notes.htm)

There is a probe (cantilever plus a tip at its end), which scans the surface of the sample. Piezoelectric ceramics move the cantilever over the surface of the sample. The cantilever bends as a response to variations of the surface topography. Since there is a laser beam being directed to the cantilever, this bending is detected optically, because the bending will cause the deflection of the beam, which hits a photodetector after hitting the cantilever. The photodetector output will be directly proportional to that deflection. As a final result, a three dimensional image of the surface is obtained.

Hook's law allows determining the force of the interaction between the tip of the cantilever and the sample (F), given the cantilever spring constant (k') and the deflection of the cantilever (Δ):

$$F = -k' \times \Delta \qquad (2.1)$$

AFM can be operated in contact mode or in tapping mode. When AFM is operating in contact mode, a fixed initial height of the probe over the sample is defined, and consequently the cantilever will have a constant initial deflection. The probe glides over the sample, and so the force of the interaction between the tip and the sample can be determined using the cantilever spring constant, the deflection of the cantilever, and Hook's law. The contact mode may damage samples which are not completely immobilized, and soft samples.

In tapping mode, more often used for biological samples, the cantilever oscillates with a free amplitude, for example by means of a piezoelectric ceramic. The amplitude and phase of the oscillations change as a result of the contact between the tip and the surface, and that is the basis of the formation of the image.

In this experimental work, AFM was performed in air and in water, in tapping mode, with a Veeco Multimode Nanoscope 4A and a Nanoscope III Multimode SFM (Digital Instruments / Veeco, USA), mainly for gaining knowledge of the surface porosity, as well as the surface topography, of the nanoparticles.

2.2 Confocal Laser Scanning Microscopy

Confocal laser scanning microscopy is a microscopy technique for obtaining high-resolution optical images of serial optical sections of the specimens. Regarding nanocapsules' fabrication and study, this technique is the tool of choice, since it allows the observation of successive focal plans of the nanocapsules, giving an insight on the thickness of the polymer layers, as well as the encapsulated material (Silvano *et al.*, 2002).

The analysis of only a single focal plane of the specimen at a time is possible because of a pinhole placed in front of the detector, which filters the reflected light that comes from the specimen. The pinhole has a rather narrow aperture, so only the light from the microscope focal plane is able to pass through it and, consequently, hit the detector and be imaged. The detector images a single point at a time. The light that comes either from above or below the focal plane is physically blocked by the pinhole. This enables the in-depth analysis of thick specimens.

The light source consists of a laser beam, directed towards an objective which focuses this light to a single point in a given focal plane of the specimen. Two galvanometric scanners deflect the laser beam in the X and Y directions, thus enabling the line-by-line scanning of the specimen. The microscope stage is moved up and down by a computer-controlled fine-step motor, allowing the focal plane to be selected.

When the light hits the specimen, it excites fluorescence, and this radiation is collected by the objective, and directed towards the detector through a dichroic beam splitter. The intensity of that fluorescent light is directly proportional to the intensity of the resulting pixel in the image (figure 2.2).

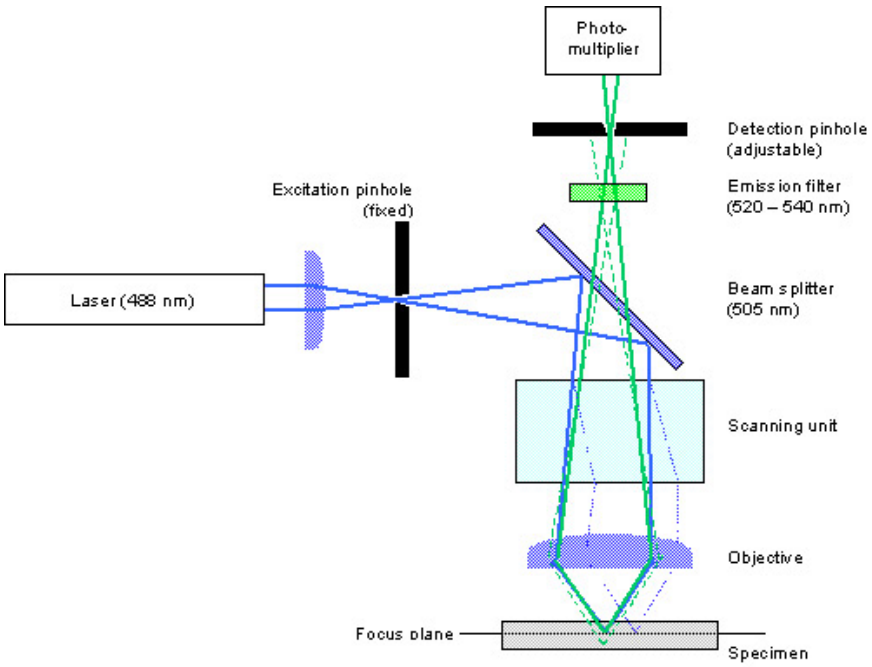

Figure 2.2 - The components of a confocal laser scanning microscope (retrieved from http://www.uk.plbio.kvl.dk/~als/confocal.htm)

The use of a laser beam as a source of light and a photomultiplier as a detector is advantageous, since they allow to perform a pointwise illumination of the specimen, and to obtain a significant output signal even if the amount of light in the final image is reduced due to the confocal filtering.

During this experimental work, confocal laser scanning microscopy was used to study the fluorescently-labeled colloidal particles, as well as to assess the encapsulation efficiency of the fluorescently-labeled therapeutic molecules. It was performed with the Laser Scanning Confocal Microscope Leica SP2 AOBS (Leica Microsystems, Germany).

2.3 Dynamic Light Scattering

Dynamic light scattering is a technique for measuring, in a non-invasive way, the hydrodynamic radius of nanoparticles and molecules, such as colloids and polymers, dispersed or dissolved in a liquid (Degen *et al.*, 2008).

This technique uses the Brownian motion of the particles to determine their size. In a suspension, solvent molecules, due to their thermal energy, are in motion. The Brownian motion is a result of collisions of solvent molecules with particles in suspension. If a suspension of particles is irradiated by a light source, e. g. a laser, each moving particle hit by that light will scatter it in all directions (figure 2.3).

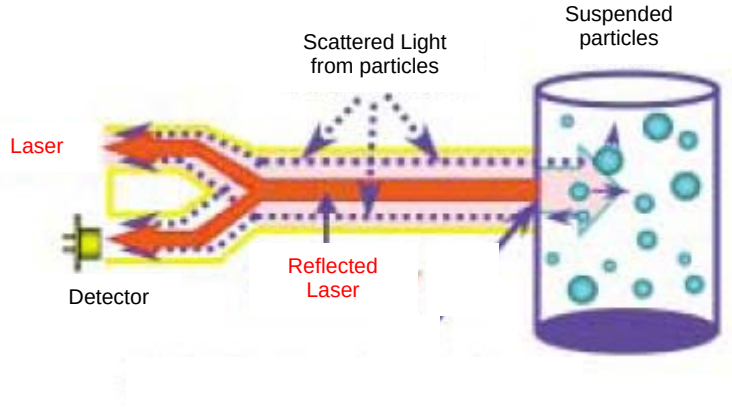

Figure 2.3 - The principle of particle size measurement by DLS (retrieved from http://www.microtrac.com/downloads/2006/Nano(US)Web.pdf)

The fluctuation of the intensity of the scattered light will depend on the size of the particles. In fact, larger particles undergo slow Brownian motion, while smaller particles undergo fast Brownian motion. Consequently, in the presence of large particles, the intensity of the scattered light will suffer bigger and slower intensity fluctuations, while in the presence of small particles it will suffer smaller and faster intensity fluctuations.

The analysis of those fluctuations will yield the velocity of the Brownian motion of the particles. The particle size can be obtained from that velocity.

The diameter of a particle depends on the concentration and type of ions in the medium, as well as the size of the particle "core" and any structure present on the surface of the particle. This features influence also the way a particle diffuses in a fluid.

The Stokes-Einstein relationship allows the calculation of the hydrodynamic averaged intensity radius (R_H), from the diffusion coefficient (D), and consequently to determine the particle size:

$$R_H = \frac{kB \times T}{6\pi \times \eta 0 \times D} \tag{2.2}$$

where R_H is the radius of a hard sphere that diffuses at the same rate as the particle under examination, $\eta 0$ is the viscosity of the medium, k_B is the Boltzmann Constant and T is the absolute temperature. This relation is valid only for spherical monodisperse particles.

DLS was used throughout the experimental work to assess the size distribution of CS:GA nanoparticles. It was performed with a ZetaSizer Nano Series Nano-ZS Model ZEN3600 (Malvern Instruments Limited, Worcestershire, UK).

2.4 Electrophoretic Mobility

The electrophoretic mobility method was used for measuring the zeta potential of the nanoparticles and nanocapsules.

When particles are part of a dispersion in an aqueous medium, they suffer ionization of their surface groups, or adsorption of charged species. As a result, they acquire a surface charge, which is responsible for the formation of a layer around the particle which is different from the bulk solution. This layer becomes an effective part of the particle

itself, and moves along with the particle when it undergoes Brownian motion. The zeta potential is the potential at the borderline between this layer and the bulk of the solution, and is a measure of the magnitude of the repulsion or attraction between particles (Xu, 2008) (figure 2.4).

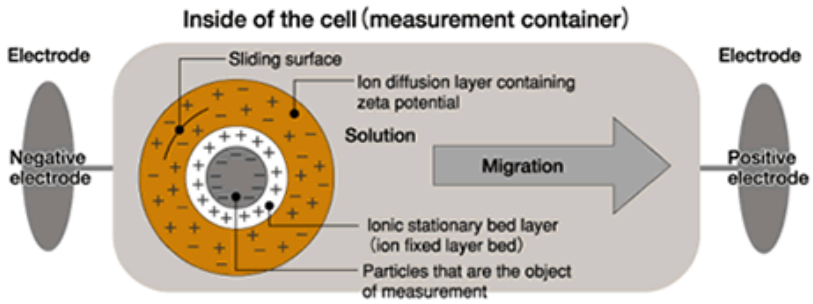

Figure 2.4 - The various layers that form around a given particle in an aqueous dispersion (retrieved from http://www.lenntech.com/zeta-potential.htm)

The principle of the electrophoretic mobility method is the application of an electric field across a given dispersion, causing the particles to migrate towards the electrode whose charge is opposite to their zeta potential, with a velocity which is proportional to its magnitude (figure 2.5).

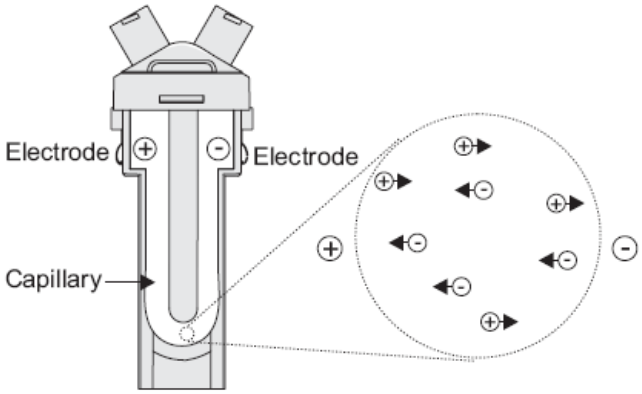

Figure 2.5 - The electrophoretic mobility method for measuring zeta potential (retrieved from http://www.nbtc.cornell.edu/facilities/downloads/Zetasizer%20chapter%2016.pdf)

If a laser beam is directed towards the dispersion, the moving particles cause its frequency to phase shift, which is measured as the particle mobility. By inputting the

dispersant viscosity, and applying the Smoluchowski (Smoluchowski, 1903) or Huckel (Huckel, 1924) theories, one can convert the particle mobility to zeta potential. Both the Smoluchowski theory and the Huckel theory relate the electrophoretic mobility of the particles to their zeta potential, the viscosity of the solvent and the dielectric constant of the dispersion medium. The former is used for high ionic strengths, while the latter is applied to low ionic strengths.

ZP measurements were performed using the same apparatus used for the dynamic light scattering measurements.

2.5 Transmission Electron Microscopy

Transmission electron microscopy is a microscopy technique based on the interaction of an electron beam with a given specimen. Since the electrons interact with single atoms, providing that the specimen is in an ultra thin state, this technique has a much higher resolution than light microscopy, making it very useful in the analysis of both biological and inorganic samples. A schematic representation of a transmission electron microscope can be seen in figure 2.6.

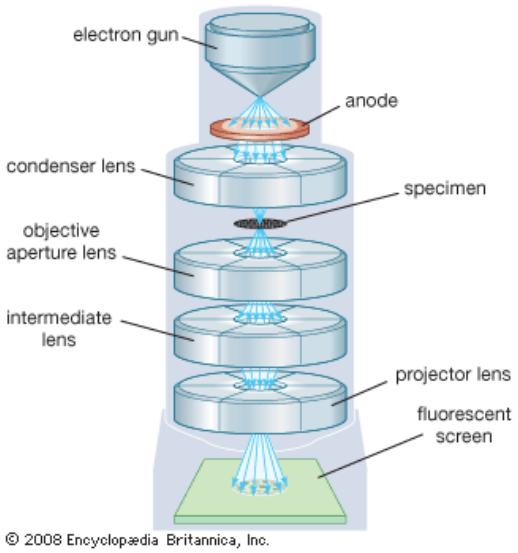

Figure 2.6 - Schematic representation of a transmission electron microscope (retrieved from http://www.britannica.com/EBchecked/topic-art/183561/110686/Transmission-electron-microscope)

There is an emission source, generally a tungsten filament, which emits electrons when it receives electric current from a high voltage source. Electrons travel in a vacuum system. Condenser lenses subsequently form the electron beam, which can be manipulated using a combination of magnetic and electrostatic fields. This way, the focusing power is controlled. Objective lenses are responsible for focusing the electron beam on the sample, and the distance between the image plane of the objective lenses and the sample defines TEM's magnification.

Samples are typically deposited on support grids made of Cu, that possess an ultramicrotomy mesh. Their dimensions are most frequently 3 mm of diameter, 100 μm of edge thickness, and they are electron transparent in the mesh region. Uranyl acetate is generally used as a negative staining for samples of biological origin. Since it deposits uranium atoms in specific regions of the specimen, that way absorbing electrons from the beam, it enhances the contrast, facilitating the imaging.

A fluorescent screen is responsible for TEM imaging, which can also be coupled to a photographic film, or an image recording system. Projector lenses expand the electron beam onto the imaging device.

TEM samples were stained with uranyl acetate 1% solution, and placed on copper grids prior to imaging. The images were obtained on a TEM Zeiss model 902C, 80 KV.

2.6 Turbidity measurements

The formation of a complex by means of coacervation of two polymers can be followed by turbidimetric measurements, since the turbidity (τ) of the equilibrium phase is related to the formation of a non-soluble phase (Espinoza-Andrews *et al.*, 2007). The greater

the amount of macromolecules in the solution, the higher the τ (Espinoza-Andrews *et al.*, 2007).

Hajdu and colleagues determined the τ of nanoparticles prepared by self-assembly of CS and poly-γ-glutamic acid using the following relationship:

$$\tau = \left(\frac{-1}{L} \right) \ln \left(\frac{I_t}{I_0} \right) \quad (2.3)$$

where L is the light path length in the cell (1 cm), I_t is the transmitted light intensity, and I_0 is the incident light intensity (Hajdu *et al.*, 2008). Since L = 1 cm, τ = A. The absorbance of the samples was measured at a wavelength of 500 nm, assuming that it is equivalent to the τ of the samples. The measurements were made using a BioTek Synergy 2 fluorimeter (BioTek Instruments, USA).

3 The poly(L-lysine)/poly(L-glutamic acid) system

3.1 Introduction

Poly(L-lysine) (PLL) and poly(L-glutamic acid) (PLG) have been used to produce multilayered films by layer-by-layer deposition (Pradier *et al.*, 2007), since they are oppositely charged polymers at neutral pH (Zhao *et al.*, 2006). They are polypeptides of lysine and glutamic acid, respectively (figures 3.1 a) and b)). The pK_a of PLG in solution is close to 4.2, decreasing to approximately 2.5 in an immobilized film, while the pK_a of PLL in solution lies around 9, increasing in the immobilized film (Pradier *et al.*, 2007). The deposition of these polyelectrolytes on substrates makes them stronger polyelectrolytes (Zhi and Haynie, 2004).

a) b)

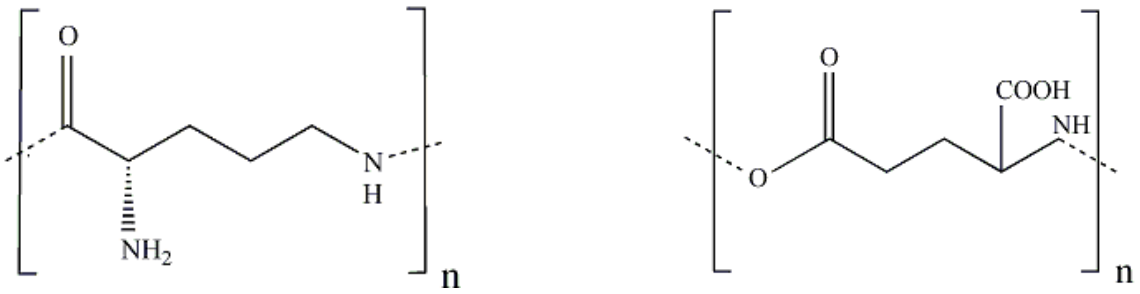

Figure 3.1 - a) Poly(L-lysine) and b) Poly(L-glutamic acid)

PLL has basic amine groups on its side chain (Pradier *et al.*, 2007). At physiological pH, the ε-amino groups of each monomer are protonated, thus PLL is positively charged under these conditions (Mintzer and Simanek, 2009; Pradier *et al.*, 2007). PLL is a valuable vehicle for gene transfer being one of the most studied cationic polymers for

DNA delivery due to its ability to condense DNA (Jeong *et al.*, 2007; Mintzer and Simanek, 2009; Morille *et al.*, 2008).

PLG is produced by several species of the genus *Bacillus*, being an exocellular capsular polymer of these microorganisms. PLG can also be used for drug and protein delivery applications (Richard and Margaritis, 2001). For example, glucose oxidase, pre-adsorbed to $CaCO_3$ template particles, was successfully encapsulated through the subsequent stepwise adsorption of PLL and PLG onto the templates (Zhi and Haynie, 2006). At intermediate values of pH, the carboxylate groups of PLG are negatively-charged (Pradier *et al.*, 2007). Consequently, at physiological pH values, PLL and PLG are both fully ionized, possessing one charge per monomer (Zhi and Haynie, 2004). Because of their peptide structure, PLL and PLG have a biodegradable nature, which is an advantage for *in vivo* use.

It is known that polyelectrolyte multilayer (PEM) films have potential applications as bioactive coatings displaying time scheduled biological activity (Jourdainne *et al.*, 2007). If the principle that is inherent to the production of these films on planar surfaces is applied to the coating of colloidal particles, the use of their high specific surface becomes possible, resulting in several advantageous applications, such as the adsorption or entrapment of drugs (Sukhorukov *et al.*, 2005). This way, the potential ability of planar films composed of polyaminoacids such as PLL and PLG to deliver biomolecules to cells (Jourdainne *et al.*, 2007) might be present in nanoparticles and nanocapsules of the same polymers, possessing entrapped and/or encapsulated active molecules. These systems could potentially display the additional advantage of permitting a more selective action of the delivered molecules, since they could be internalized only by the cells of interest.

In this work, PLL/PLG nanoparticles and nanocapsules were prepared by the layer-by-layer technique, involving the consecutive deposition of the oppositely charged polypeptides onto polystyrene (PS) colloidal particles. Nanocapsules were produced by removing the PS cores at the end of the process (figure 3.2).

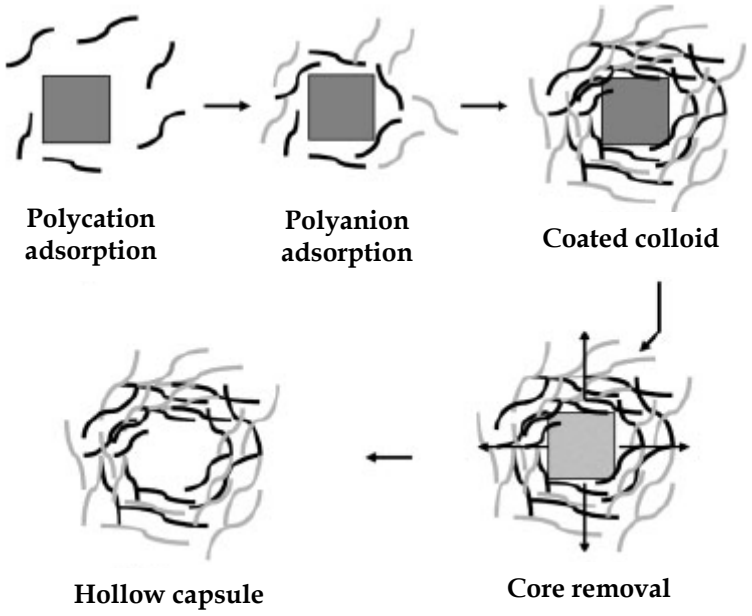

Figure 3.2 - Schematic representation of the LbL technique (adapted from Donath *et al.*, 1998)

The systems were used to entrap and encapsulate a beta-sheet breaker peptide, with the sequence -Leu-Pro-Phe-Phe-Asp- (iAβ5) indicated by Estrada and Soto (Estrada and Soto, 2006). Given the fact that peptides generally suffer a rapid degradation in biological fluids, this carrier may increase the half-life time of iAβ5 and improve its stability.

3.2 Polymers used

Poly(L-lysine) hydrobromide (one HBr / residue), with a molecular weight of ~70,000 and a degree of polymerization of 327 (viscosimetry), and poly(L-glutamic acid) sodium salt, with a molecular weight of ~21,000 and a degree of polymerization of 136

(viscosimetry), were purchased from Sigma. Poly(allylamine hydrochloride), with a molecular weight of ~56,000, and poly(sodium 4-styrene sulfonate), with a molecular weight of ~70,000, were purchased from Sigma.

3.3 Preparation of PLL/PLG nanoparticles and nanocapsules

3.3.1 Nanoparticles

PLL/PLG nanoparticles were produced following the LbL technique. A few variations were studied, differing on the succession and number of added layers. All of them kept the colloidal templates (PS cores with a diameter of 1.06 ± 0.03 μm). "PS/$(PLL/PLG)_6$" and "PS/$(PLL/PLG)_5$/PLL" nanoparticles were prepared with polypeptide solutions of 5 mg/mL. The suitable masses of the two polymers, PLL and PLG, were dissolved in PBS (0.01 *M* of phosphate buffer, 0.0027 *M* potassium chloride, 0.137 *M* sodium chloride and a pH of 7.4 at 25 ºC; Sigma). PS cores (50 μL) (microparticles GmbH, Berlin, Deutschland) were first washed with ultrapure water (resistivity of 18.3 MΩ.cm, obtained from distilled water using an EASYpure RF apparatus) in a 1.5 mL microcentrifuge tube, by centrifugation (Eppendorf Centrifuge 5804 R, Eppendorf AG, Hamburg) under the following conditions: 5000 rpm, 5 min., 20 ºC. The resulting supernatant was discarded. The washing procedure was repeated three times. Afterwards, 1 mL of the PLL solution was added to the PS cores. Following resuspension, the contact between the polymer solution and the cores was promoted through mild agitation for 20 minutes. Then, centrifugation under the same conditions mentioned above was carried out, followed by the discard of the supernatant and two washing steps. The subsequent PLG layer was added following the same procedure.

This way, the desired number of polymeric layers of alternately opposite charges was added, the outermost layer being PLG (PS/(PLL/PLG)$_6$ nanoparticles) or PLL (PS/(PLL/PLG)$_5$/PLL nanoparticles).

For the production of labeled particles, PLL-FITC (molecular weight of 68,300; degree of substitution is 7 mmoles of FITC per mole of lysine monomer; Sigma) was added instead of PLL. Fluorescein isothiocyanate (FITC) was used as the fluorescent molecule. Its excitation/emission wavelengths are, respectively, 494/518 nm, so the nanoparticles displayed green fluorescence when observed by confocal laser scanning microscopy (CLSM). "PS/PLL-FITC/PLG" nanoparticles were prepared by adding 100 µL of a PLL-FITC solution (PBS pH 7.4) to PS cores. Different concentrations of PLL-FITC were tested (1 mg/mL, 2.5 mg/mL or 5 mg/mL). Then 100 µL of a 2.5 mg/mL PLG solution were subsequently added to each of the three suspensions.

Labeled iAβ5 peptide (iAβ5-FITC) was entrapped in the particle polymeric walls. iAβ5-FITC (relative molecular mass 996.04, purchased from Bachem) was dissolved in acetonitrile (HPLC-gradient grade purchased from Prolabo)/ultrapure water solution, with 1% of trifluoroacetic acid (TFA, purchased from Sigma) to a final peptide concentration of 1 mg/mL. The iAβ5-FITC (1 mL) was added to either following a PLG layer (PS/(PLL/PLG)/iAβ5-FITC/(PLL/PLG) nanoparticles) or a PLL layer (PS/(PLL/PLG)/PLL/iAβ5-FITC/(PLL/PLG)$_3$ nanoparticles). In both cases, several PLL and PLG layers were added subsequently to iAβ5-FITC layer.

PS/(PLL/PLG)/iAβ5-FITC/(PLL/PLG) nanoparticles were tested at pH 3 and 10. Nanoparticles suspensions were allowed to rest for a few days, followed by the discard of the supernatant and addition of pH 3 (citric acid ~ 0.040 *M*; sodium hydroxide ~0.021 *M*; sodium chloride ~ 0.060 *M*; purchased from Sigma) or pH 10 (sodium tetraborate ~ 0.013 *M*; sodium hydroxide 0.018 *M*; purchased from Sigma) buffer

solutions. CLSM analyses were performed two days and one week after adjusting the pH, and also after submitting them to ultrasounds, to determine the stability of the nanoparticles.

3.3.2 Nanocapsules

PLL/PLG nanocapsules were prepared following the same procedure described in section 3.3.1, regarding the concentration of polyelectrolyte solutions and washing steps. PS cores with a diameter of 1.06 ± 0.03 μm were used as templates for the successive deposition of PLL and PLG. The desired number of polymeric layers of alternately opposite charges was added. After the washing steps of the last added layer (PLG), the dissolution of the PS cores was performed, after centrifugation and discharge of the supernatant, by adding 1 mL of tetrahydrofuran (THF) (Sigma). THF was then removed by letting the nanocapsules sediment with time and substituting the supernatant by ultrapure water. This rinsing step was repeated for several days.

In order to permit visualization of the nanocapsules by CLSM, the second last added polymeric layer consisted of PLL-FITC. With that purpose, 1 mL of a PLL-FITC 5 mg/mL solution (in PBS pH 7.4) was added to the nanocapsules. Nanocapsules of PAH/PSS polymers were also performed and used to encapsulate the iAβ5-FITC. iAβ5-FITC solution was prepared according to the procedure indicated in section 3.3.1. The permeability of the capsules was controlled by adjusting the pH with a citric acid ~ 0.040 *M*; sodium hydroxide ~ 0.021 *M*; sodium chloride ~ 0.060 *M* buffer solution (pH 3) and a sodium tetraborate ~ 0.013 *M*; sodium hydroxide 0.018 *M* buffer solution (pH 10), both purchased from Sigma.

3.4 Characterization of PLL/PLG nanoparticles and nanocapsules

The LbL assembly of PLL/PLG was followed by zeta potential measurements, after the washing steps following the deposition of each layer. The nanosystems with a fluorescently labeled layer were additionally characterized by confocal microscopy.

Figure 3.3 depicts the ZP values after the addition of each polypeptide layer to PS cores. The resulting nanoparticles had 12 layers, with PLL as the first added layer and PLG as the outermost one. The ZP signal inversion after the addition of each layer suggests the successful deposition of the oppositely charged polymers. It is also of note that the ZP values range generally from 36 ± 2 mV for PLL layers to -14 ± 7 mV for PLG layers. This indicates that the charge excess generated at the outermost layer remains constant (Lavalle *et al.*, 2002).

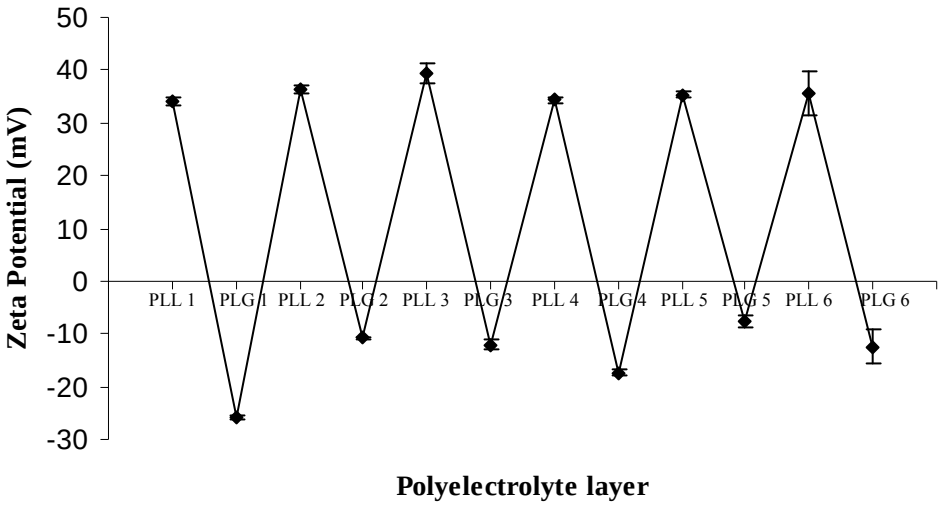

Figure 3.3 – Zeta Potential of the successive PLL and PLG polyelectrolyte layers added to PS cores by the LbL technique.

The shape and integrity of the nanoparticles were assessed by confocal microscopy using labeled PLL layer. In this case, the first layer added was PLL-FITC, followed by PLG (PS/PLL-FITC/PLG nanoparticles, see section 3.3.1). Deposition of labeled PLL was performed at three different concentrations (1, 2.5 and 5 mg/mL), to study the

influence of this parameter on ZP value and particle integrity. The ZP of all PLL-FITC layers was around 15 ± 5 mV. The subsequently added PLG layers, deposited through the addition of 100 μL of a PLG 2.5 mg/mL solution, displayed a ZP value of about -30 mV for all cases. The results indicate that ZP values do not significantly differ when using increasing concentrations of the starting PLL-FITC solution for the first layer deposition. The ZP values suggest that there is a complete coverage of the PS core already at the lowest concentration tested. The analysis of figure 3.3 indicates that the absolute ZP values of non labeled PLL are higher than those of fluorescently-labeled PLL. PLL-FITC is a polymer composed of lysine monomers, having FITC residues linked to a certain amount of lysine monomers (each FITC residue is linked only to a single lysine). The PLL-FITC used in this experience had a degree of substitution of 7 mmoles of FITC per mole of lysine monomer. Since the linkage between FITC and lysine is established between the carboxyl group of FITC and the ε-amino group of the lysine monomer, PLL-FITC possesses less positive charges than PLL.

Figure 3.4 a) – c) presents CLSM images of PS/PLL-FITC/PLG nanoparticles. It can be seen that aggregation of the nanoparticles increased with the concentration of PLL-FITC layer. This might be explained by the capacity of weakly bond PLL chains to diffuse "out" of the film (Lavalle *et al.*, 2002). One can speculate that higher concentrations of the PLL-FITC layer applied meant a higher number of FITC residues on the surface of the nanoparticles. Jessel and colleagues built, under similar conditions to the ones used in this experimental work, namely in what concerns to pH and NaCl concentration, a PEM film consisting of the alternate deposition of PLG and PLL, with protein A embedded after the third polyelectrolyte layer. On the top of that film, as the outermost layer, PLL-FITC was deposited (Jessel *et al.*, 2003). CLSM observations of a vertical section of the multilayered film showed that green fluorescence, attributable to

PLL-FITC, was visible over the whole thickness of the film, indicating that PLL-FITC diffused through the 41 polymeric layers below it, until it reached the substrate (Jessel *et al.*, 2003). These authors have thus demonstrated the vertical diffusion of PLL when included in a PEM film along with PLG. The results presented in figure 3.4 a) – c) agree with those of Jessel and colleagues, and were expectable in the light of the findings of those authors. The particles had a spherical shape, with diameters of around 1 μm, and had an integral wall.

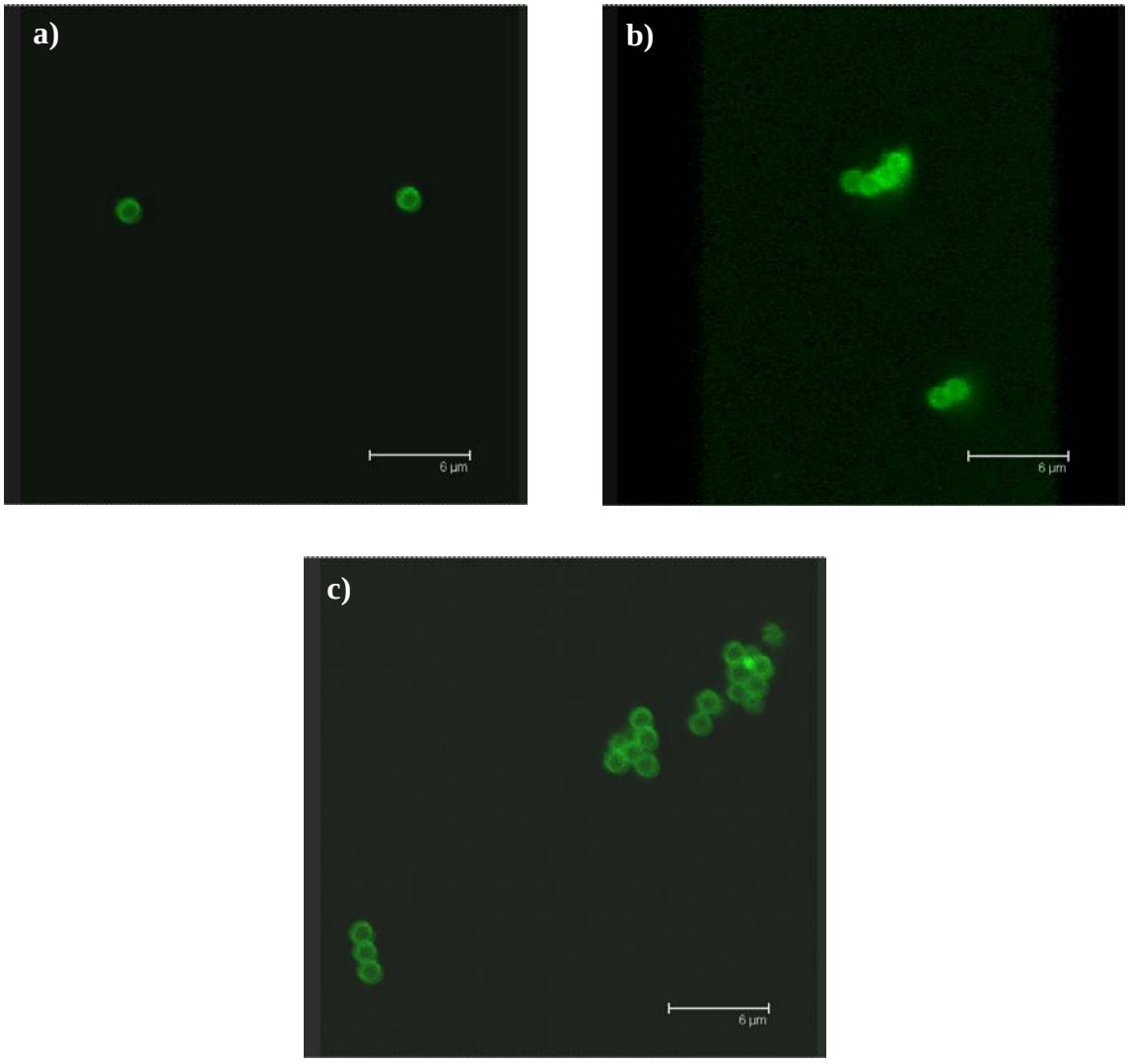

Figure 3.4 – CLSM images of PS/PLL-FITC/PLG nanoparticles. The PLL-FITC layer was deposited through the addition of PLL-FITC solutions with a concentration of a) 1 mg/mL; b) 2.5 mg/mL and c) 5 mg/mL. In all the three cases, a PLG layer was subsequently deposited through the addition of a PLG solution with a concentration of 2.5 mg/mL. The scale bars represent 6 μm.

The vertical diffusion of PLG when included in a PEM film along with PLL was also previously demonstrated by Lavalle and colleagues (Lavalle *et al.*, 2004). These authors confirmed, by CLSM observations, the vertical diffusion of PLL-FITC and of PLG labeled with the Alexa Fluor 594 probe, which emits red fluorescence at 690 nm (Lavalle *et al.*, 2004). These findings confirmed the results obtained by Jessel and colleagues.

PEM films built under the conditions above indicated can follow two types of growth, namely linear or exponential growth (Jourdainne *et al.*, 2007; Lavalle *et al.*, 2004). Linear growth is typical of PEM films composed of synthetic polyelectrolytes (Jourdainne *et al.*, 2007), the pair PAH/PSS being the most representative among them (Jourdainne *et al.*, 2007; Lavalle *et al.*, 2002; Lavalle *et al.*, 2004). In this type of PEM, the thickness and the amount of polyelectrolytes deposited per bilayer increase linearly as a function of the number of deposited bilayers (Jourdainne *et al.*, 2007).

PEM films composed of natural polyelectrolytes follow a typical exponential growth (Jourdainne *et al.*, 2007). PLL and PLG are among the polyaminoacids that show this type of growth (Jourdainne *et al.*, 2007; Lavalle *et al.*, 2004). Exponential growth of PEM films is characterized by the exponential increase of both the thickness and the amount of polyelectrolytes deposited per bilayer, as a function of the number of deposited bilayers (Jourdainne *et al.*, 2007). This type of growth is made possible when one of the two polyelectrolytes involved is capable of diffusing “in” and “out” of the film, during the deposition of each layer (Lavalle *et al.*, 2004). As shown above, in what concerns to the PLL/PLG pair, both the polyelectrolytes are capable of that type of diffusion, and they share that feature due to their biological nature (Lavalle *et al.*, 2004). Thus, the PLL/PLG pair can be regarded as a representative example of exponential growth, when applied to PEM films. Indeed, the exponential growth of that

polyelectrolytic pair was demonstrated and explained before (Lavalle *et al.*, 2002). The authors built, under experimental conditions very similar to those followed in this work, PEM films containing several (PLG/PLL) bilayers, applied over an initial PEI precursor layer (Lavalle *et al.*, 2002). They demonstrated that both the thickness and deposited polyelectrolyte mass of PLG/PLL PEM films increased in a superlinear way, as a function of the number of bilayers, while PAH/PSS PEM films had a linear increase of the same variables, reaching values of thickness and deposited mass much lower than those of PLL/PLG PEM films (Lavalle *et al.*, 2002). As a nuclear assumption for the understanding of the mechanism of formation of PLL/PLG PEM multilayers, the authors proposed that, among the polyelectrolytic chains forming the outermost layer of a multilayer, the existence of two kinds of chains should be considered: those strongly interacting with the layer immediately below, effectively taking part in the whole film, and those weakly bond to the structure of the film (Lavalle *et al.*, 2002). Thus, when for example a PLG solution comes in contact with a PEM film whose outermost layer is PLL, weakly bond PLL chains diffuse out of it. After that, PLG chains diffuse into the film, and as long as there is an excess of PLG chains in solution, the compensation of charges is effective, and the film acquires a negative surface charge. When afterwards this film comes in contact with a PLL solution, weakly bond PLG chains diffuse out of it, followed by the diffusion of PLL chains into the film. If the PLL solution has an excess of PLL chains, there will be compensation of charges, conferring the film a positive surface charge. The repetition of these steps leads to the formation of exponentially growing PLL/PLG PEM films (Lavalle *et al.*, 2002).

By suggesting the diffusion of PLL chains "out" of the film, the work of Lavalle and colleagues (Lavalle *et al.*, 2002) might also be useful to understand the concentration dependent aggregation behavior observed for FITC-labeled nanoparticles (figure 3.4 a)

– c)). FITC possesses a polycyclic aromatic group, namely a xanthone group, which has three rings, two of them aromatic. A parallelism can be established between the chemical structure of FITC and that of other fluorescent dyes, like the perylenediimide derivatives. These molecules have a perylene group, which is a polycyclic aromatic group of five rings, four of them aromatic (Ribeiro *et al.*, 2009). In an experience where silica nanoparticles were doped with perylenediimide derivatives immobilized on their surface, aggregation of the dyes was reported when the nanoparticles were dispersed in water (Ribeiro *et al.*, 2009). The aggregation observed between PS/PLL-FITC/PLG nanoparticles might be attributable to the aggregation of FITC molecules present at their surface.

PLL/PLG nanoparticles with entrapped iAβ5-FITC within their polymeric layers were prepared. It has been demonstrated before that antibodies kept their biological activity when in a layer which was embedded in a PAH/PSS PEM film (Caruso *et al.*, 1997).

The ZP of the several layers of PS/(PLL/PLG)/iAβ5-FITC/(PLL/PLG) nanoparticles (see section 3.3.1) is depicted in figure 3.5.

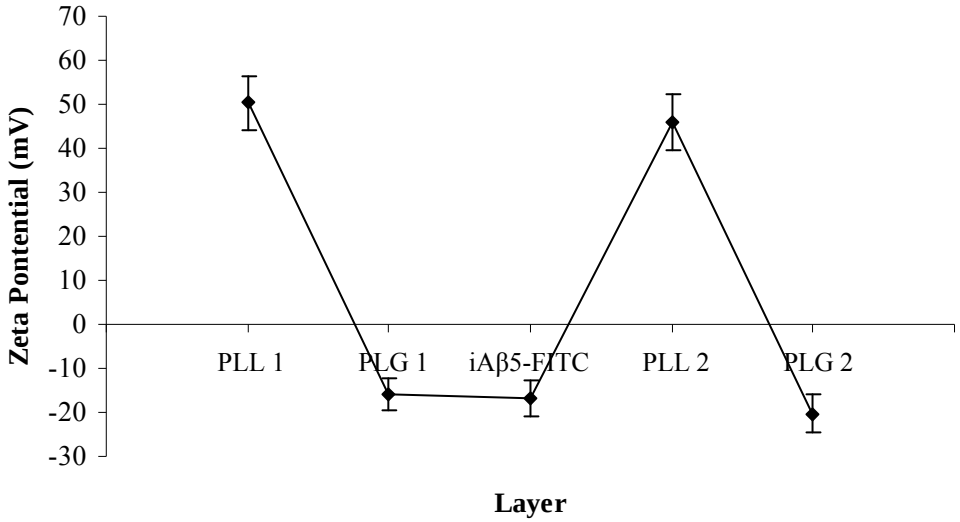

Figure 3.5 – Zeta Potential of the successive PLL, PLG and iAβ5-FITC layers used in the production of PS/(PLL/PLG)/iAβ5-FITC/(PLL/PLG) nanoparticles.

PS/(PLL/PLG)/PLL/iAβ5-FITC/$(PLL/PLG)_3$ nanoparticles (see section 3.3.1) were also studied in terms of the ZP of the successive added layers. The respective measurements are presented in figure 3.6. Higher absolute ZP values for PLL layers were always verified, supporting the data obtained for non-labeled nanoparticles (figure 3.3).

The analysis of figure 3.5 shows that the addition of the iAβ5-FITC layer caused no appreciable alteration in the negative charge of the PLG layer preceding it. In figure 3.6 there is an effective inversion of the ZP, from positive to negative values, when the iAβ5-FITC layer is added to the positively charged PLL layer.

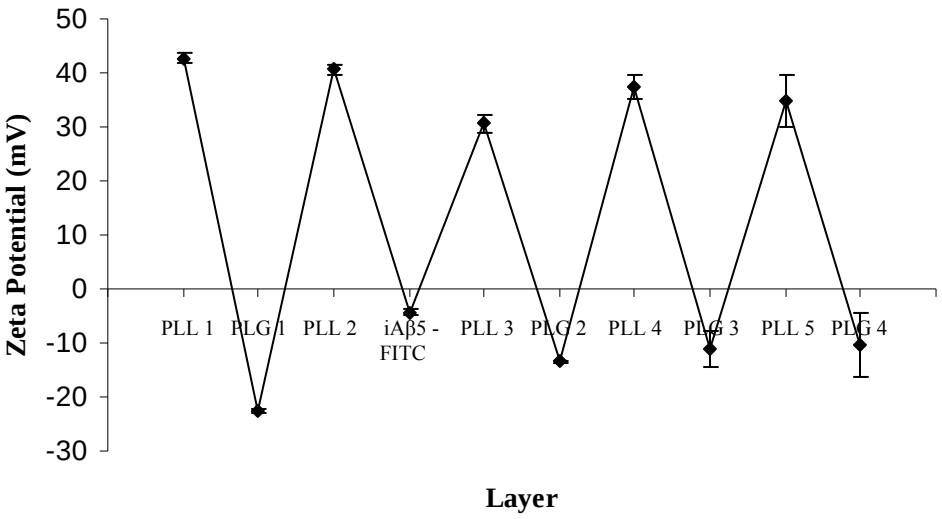

Figure 3.6 – Zeta Potential of the PLL, PLG and iAβ5-FITC layers used in the production of PS/(PLL/PLG)/PLL/iAβ5-FITC/$(PLL/PLG)_3$ nanoparticles.

The use of FITC fluorescent dye allowed visualization of the nanoparticles by CLSM (figure 3.7). We can see a reasonable number of nanoparticles, either isolated, paired or in small agglomerates, with an average diameter of about 1 μm. The integrality of their wall, indicated by the continuous fluorescence, leads to the conclusion that the peptide was successfully entrapped between the polyelectrolyte layers in both systems. These observations suggest that the lack of change in the ZP value after the addition of the iAβ5-FITC layer, which can be seen in figure 3.5, might be explained by the fact that iAβ5-FITC is negatively charged.

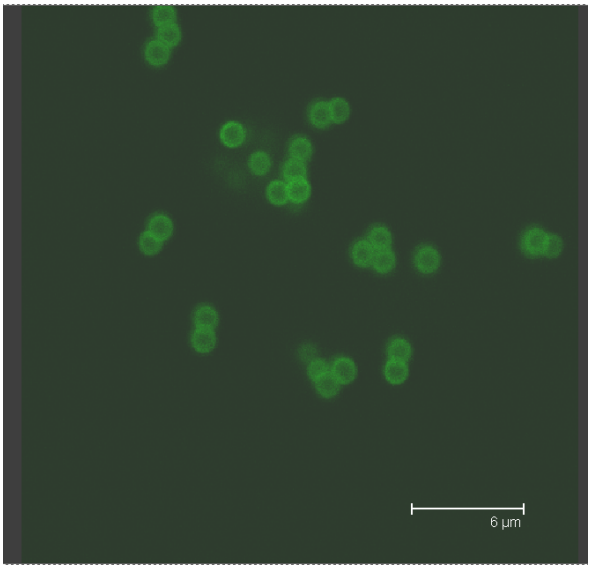

Figure 3.7 – CLSM image of PS/(PLL/PLG)/iAβ5-FITC/(PLL/PLG) nanoparticles. The scale bar represents 6 µm.

Taken together, the ZP studies and the confocal microscopy image of figure 3.7 indicate that there is an efficient adsorption of the peptide, despite the charge of the polymeric layer preceding it. In a previous study, Ladam and colleagues investigated the deposition and adsorption of several proteins on PEM films composed of PAH and PSS (Ladam *et al.*, 2001). In particular, the referred study used two kinds of proteins, either negatively or positively charged under pH 7.35 (Ladam *et al.*, 2001), a value very similar to the one used in the present work (pH 7.4). The authors found that both positively and negatively charged proteins adsorbed on either negatively or positively charged PEM films (Ladam *et al.*, 2001). Although, larger amounts of proteins were adsorbed, leading to thicker protein films, when the proteins and the outermost polyelectrolyte layer had opposite charges (Ladam *et al.*, 2001). Proteins adsorbed to PEM films ending with the same charge as theirs formed typically a monolayer, while proteins adsorbed to PEM films ending with a charge opposite to their charge formed multilayers (Ladam *et al.*, 2001). The authors suggested that adsorption of proteins onto PEM films with similar charge might be due to some polymer chains of opposite charge to the last layer that can emerge at the surface of the PEM films, facilitating the

adsorption of proteins with the same charge as the last layer (Ladam *et al.*, 2001). As stated before, diffusion of PLL and PLG on PEM films has been demonstrated (Lavalle *et al.*, 2002). Taking also into account the work of Ladam and colleagues, polypeptide diffusion might explain the adsorption of iAβ5-FITC at both PLL and PLG layers.

It is known that altering the pH of the medium is one of the most important factors for tuning the permeability of nanocapsules, namely PAH/PSS capsules (Sukhorukov *et al.*, 2005). In this polymeric system, acidic pH values (<6) create pores in the polyelectrolyte walls, allowing the encapsulation of molecules, while alkaline pH values (>8) reseal the pores and prevent the release of the encapsulated material (Antipov *et al.*, 2002; Sukhorukov *et al.*, 2005). Moreover, in a previous study, Zhi and Haynie have investigated the changes in the structure of a PEM film composed of PLL and PLG, induced by pH shifts (Zhi and Haynie, 2004). It was suggested that, at pH 7.4, the most significant secondary structure present in PLL/PLG films is the β-sheet structure (~50% of the content), while α-helix structure represented only ~5% (Zhi and Haynie, 2004). Upon exposure of the film to acidic pH 2.0 solution for 10 minutes, the content of α-helix structure increased markedly to ca. 60%, with a significant decrease of the β-sheet content, while the optical mass and the overall thickness of the film also decreased (Zhi and Haynie, 2004). The same effects on the relative contents of the secondary structures, on the optical mass and on the overall thickness of the film were observed when the film was exposed to pH 12.0 for 10 minutes (Zhi and Haynie, 2004). According to the same authors, the described reorganizations in secondary structure and mass losses are due to the charge neutralization of the polypeptidic chains that occur under extreme values of pH (Zhi and Haynie, 2004). Highly acidic or alkaline pH values decrease the number of charged groups in the film, through protonation of carboxylate groups of PLG in the first case, and deprotonation of NH_3^+ groups of PLL in the second

case. This leads to the weakening of ionic interactions between β-sheets present in adjacent layers, which in turn promotes the transition from this secondary structure to α-helix (Zhi and Haynie, 2004). At the same time, secondary structure reorganizations determine a partial dissociation of polypeptide complexes in the film, leading to the rapid mass losses observed upon exposure to both acidic and alkaline pH values (Zhi and Haynie, 2004). As an additional outcome of the reorganizations in the film, an increase in its porosity was also reported by the authors (Zhi and Haynie, 2004).

Taking into account these previous works, the behavior of PLL/PLG nanoparticles, with iAβ5-FITC entrapped within their polymeric layers, when exposed to acidic and alkaline pH values was studied, to assess the effect of pH shifts on the integrity of the layers. CLSM images of PS/(PLL/PLG)/iAβ5-FITC/(PLL/PLG) were collected, immediately after altering the pH values to 3 and 10 (using the pH 3 and pH 10 buffer solutions indicated before), and one week later after sonication of the nanoparticle suspensions (figure 3.8 a–d). Immediately after changing the pH to 3, it can be seen in figure 3.8 a), that the nanoparticles are spherical with membrane integrity and that they aggregate. In figure 3.8 b), which represents nanoparticles from the same preparation one week later and after applying ultrasounds, aggregation is less pronounced.

Figures 3.8 c) and 3.8 d) compare, respectively, similar nanoparticles exposed to pH 10, immediately after shifting the pH and one week later (and after submitting them to ultrasounds). Again, it is noticeable that the aggregation is practically inexistent among nanoparticles, one week after pH change and after applying ultrasounds. These results indicate that nanoparticles tend to aggregate when exposed to acidic or alkaline pH values. There is green fluorescence delimitating the polymeric layers of the nanoparticles in all cases, which suggests that iAβ5-FITC is still entrapped within the layers at both acidic and alkaline environments. In the light of the works of Zhi and

Haynie presented above, the possibility of a certain degree of mass loss of the outermost layers of the nanoparticles should not be neglected. However, the pH conditions used in our work (pH 3 and 10) were less drastic than those used by Zhi and Haynie (Zhi and Haynie, 2004). The midpoint of the structural transition of the film (β-sheet to α-helix) attributable to PLG occurred at ca. pH 2.9, while the same structural rearrangement of the film attributable to PLL only occurred for pH above 12 (Zhi and Haynie, 2004). Consequently, the extent of structural reorganization of the film from β-sheet to α-helix, the mass loss and the decrease in film thickness were probably smaller in our case, hence the observations of the maintenance of iAβ5-FITC entrapped in both cases.

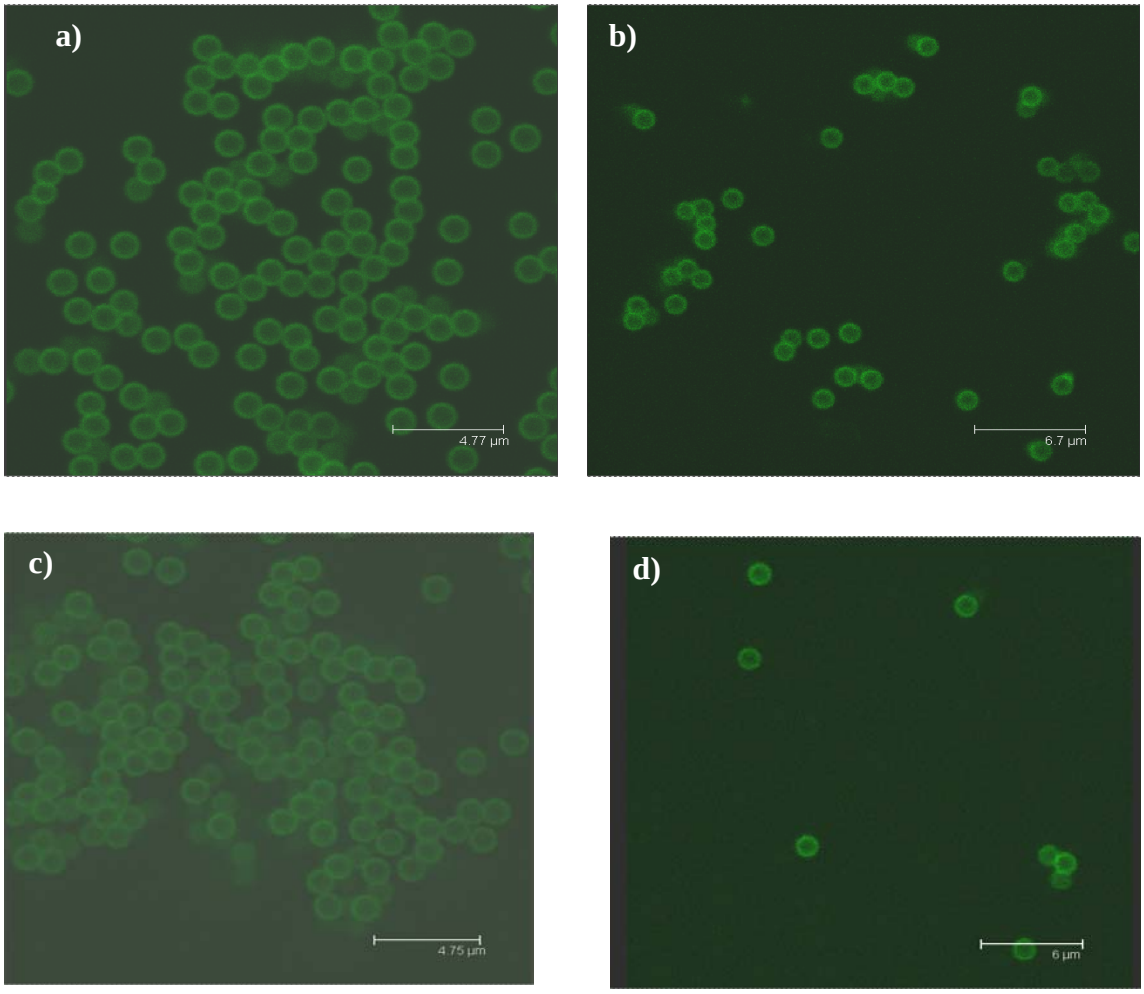

Figure 3.8 – CLSM images of PS/(PLL/PLG)/iAβ5-FITC/(PLL/PLG) nanoparticles. a) At pH = 3; b) At pH = 3, one week after pH change and after applying ultrasounds to the suspension; c) At pH = 10; d) At pH = 10, one week after pH change and after applying ultrasounds to the suspension. The scale bars represent a) 4.77 µm; b) 6.7 µm; c) 4.75 µm; d) 6 µm.

The removal of colloidal templates after the LbL deposition of the desired number of oppositely charged polyelectrolytes is the key step for the obtention of nanocapsules. The observation of PLL/PLG nanosystems after dissolution of the cores showed a high degree of aggregation among the nanocapsules (figure 3.9). The integrity of their wall was maintained, as denoted by the uniform distribution of fluorescently labeled polymer, which delimitated a non-fluorescent hollow interior. It is also of note that despite the removal of the PS cores the capsules maintain their tendentiously spherical shape and their original average diameter (~1 μm).

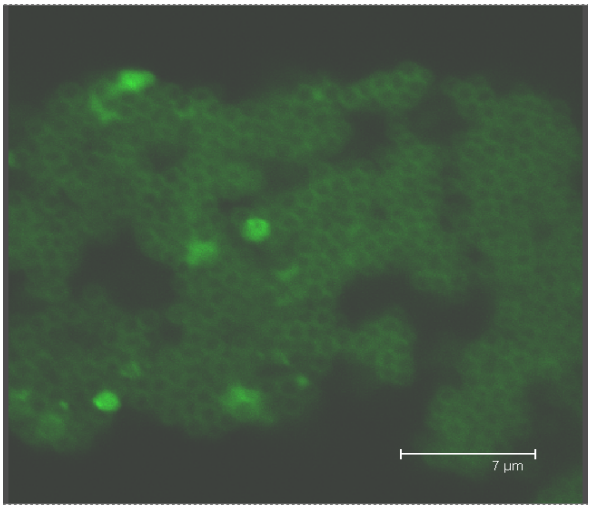

Figure 3.9 – CLSM image of PLL/PLG nanocapsules, produced using PS cores with 1 μm of diameter, and having 12 polyelectrolyte layers. The outermost layer is PLG, and the second last one is PLL-FITC. The scale bar represents 7 μm.

PLL/PLG nanocapsules were also characterized by transmission electron microscopy (TEM) and atomic force microscopy (AFM). Figure 3.10 depicts the respective TEM micrograph.

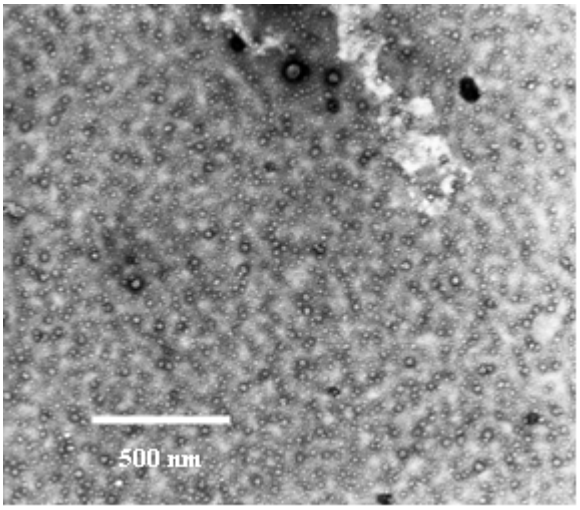

Figure 3.10 – TEM micrograph of PLL/PLG nanocapsules, produced using PS cores with 1 µm of diameter and having 12 polyelectrolyte layers. The outermost layer is PLG, and the second last one is PLL-FITC.

AFM micrographs of the nanocapsules were also collected (figure 3.11).

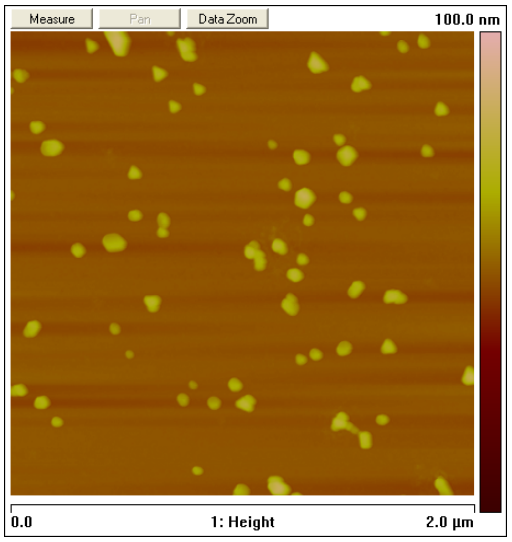

Figure 3.11 – AFM micrograph of PLL/PLG nanocapsules, produced using PS cores with 1 µm of diameter, and having 12 polyelectrolyte layers. The outermost layer is PLG, and the second last one is PLL-FITC. The height of the AFM image is represented by a vertical graded brown-light pink scale.

The analysis of figures 3.10 and 3.11 shows structures with a diameter smaller than that of the nanocapsules depicted in figure 3.9. Aktas and colleagues found that the hydrodynamic diameter of chitosan nanoparticles prepared by ionic crosslinking with TPP, was higher in liquid state than in dry state (Aktas *et al.*, 2005). The authors attributed these findings to the swelling capacity of chitosan nanoparticles in wet environments, that would consequently make them undergo a certain degree of

shrinkage when submitted to a drying operation (Aktas *et al.*, 2005). Since CLSM imaging is typically performed in a wet environment, it is possible that the diameter differences found by CLSM and TEM/AFM are due to capsule swelling/shrinking behavior in wet/dry environments. Moreover, the fact that nanocapsules have a hollow interior might be an additional factor for their shrinking in dry environments, since they lack a supporting structure, such as the PS cores, that could prevent the collapse of their shell. This phenomenon was observed by authors such as An and colleagues (An *et al.*, 2009).

The encapsulation of iAβ5-FITC in PLL/PLG nanocapsules would be a suitable way to protect and deliver the peptide as well as to increase its concentration within the system when comparing to the entrapment approach. However, PLL/PLG hollow nanocapsules aggregate and are not stable, as previously described. Therefore iAβ5 was encapsulated in a more stable and well characterized system, such as the one composed of positively charged poly(allylamine hydrochloride) (PAH) and negatively charged poly(sodium 4-styrene sulfonate) (PSS) (Antipov *et al.*, 2002; Johnston *et al.*, 2006). PAH/PSS nanocapsules having 12 polyelectrolyte layers were produced. As indicated in Section 3.3.2, the peptide was encapsulated by controlling the permeability of nanocapsules. In fact, it was reported that pH variations have influence on the switching between polyelectrolyte multilayer capsules' open-state and closed-state, through the creation of local defects on their walls, making them permeable to macromolecules at low pH values, and impermeable at pH values above 8, leading to encapsulation of the molecules of interest (Antipov *et al.*, 2002). So, when the iAβ5-FITC solution was added to the hollow nanocapsules, the pH 3 buffer solution triggered the opening of the polyelectrolyte shell, allowing the encapsulation of iAβ5-FITC. After a few days of rest,

the supernatant was discarded, and substituted by a pH 10 buffer solution, this way promoting the closing of the nanocapsules polyelectrolyte walls.

Figure 3.12 shows the respective CLSM image. The aggregation among the nanocapsules is clear. Besides, despite the uniform distribution of green fluorescence in the walls, its cumulative presence in the interior of the nanocapsules was verified only in few cases. Thus, few nanocapsules seem to have fully encapsulated iAβ5-FITC, as the peptide remained mainly attached only to the surface of the polymeric shells.

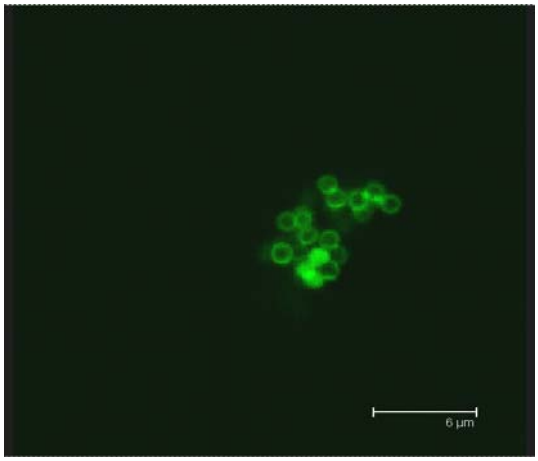

Figure 3.12 – CLSM image of PAH/PSS nanocapsules, produced using PS cores with 1 µm of diameter, having 12 polyelectrolyte layers, encapsulating iAβ5-FITC. The outermost polyelectrolyte layer is PSS. The scale bar represents 6 µm.

The results presented here suggest that nanoparticles are relatively more stable than nanocapsules, and that the entrapment of iAβ5-FITC within the polymeric layers of nanoparticles is a more efficient way of protecting the peptide than its encapsulation in the hollow interior of nanocapsules. Indeed, the adsorption of iAβ5-FITC to the polymeric layers structure of the nanoparticles was shown not to be reverted by the exposure to acidic and alkaline pH values, while nanocapsules presented stability problems (aggregation) as well as low encapsulation efficiency.

3.5 *In Vitro* studies with the SH-SY5Y cell line

The interaction of polyelectrolyte systems with neuroblastoma cells was studied by confocal microscopy to assess their cellular uptake and cytotoxicity. Since we developed the PLL/PLG system as a nanocarrier for the β-sheet breaker peptide of amyloid-β peptide (iAβ5), we chose to study the interactions of PLL/PLG nanoparticles and nanocapsules with neuroblastoma cells (SH-SY5Y cell line), given the fact that they have been used as a model cell system for studying neuronal cell death (Jung *et al.*, 2009; Junli *et al.*, 2009; Uberti *et al.*, 2002). A widefield microscopy (operating in transmission mode) image of SH-SY5Y cells is presented in figure 3.13, showing their typical fusiform morphology, characterized by the emission of neurites to the surrounding area.

Cells were plated on 4-well Lab-Tek® II Chamber Slide™ systems, and kept at 37 ºC in a humidified atmosphere composed of 95% O_2 and 5% CO_2. Cells were incubated with PLL/PLG nanoparticles containing iAβ5-FITC entrapped, and also with PLL/PLG nanocapsules having a FITC-labeled polymeric layer. CLSM observations were performed at different incubation times (15 minutes, 1 hour and 24 hours). Only after 24 hours incubation time did the nanosystems appear in the vicinity of the cellular membranes. Figure 3.14 displays a CLSM image of SH-SY5Y cells incubated for 24 hours with PS/(PLL/PLG)/PLL/iAβ5-FITC/$(PLL/PLG)_3$ nanoparticles (see section 3.3.1). Figure 3.15 depicts CLSM images of SH-SY5Y cells incubated for 24 hours with $(PLL/PLG)_5$/PLL-FITC/PLG nanocapsules, produced using PS cores with 1 μm of diameter (see section 3.3.2).

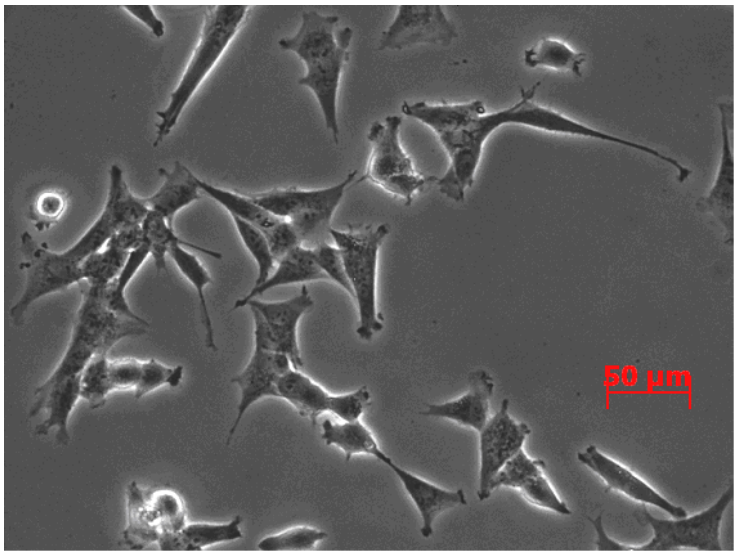

Figure 3.13 – Widefield microscopy (operating in transmission mode) image of SH-SY5Y cells

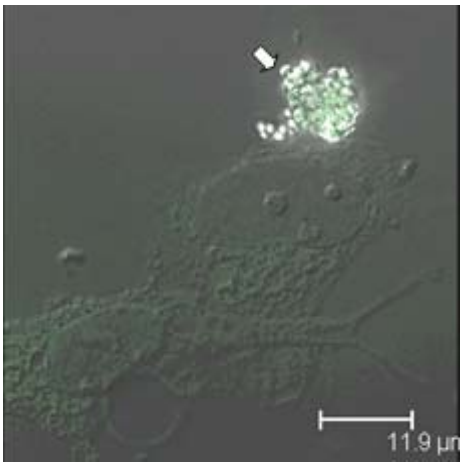

Figure 3.14 – CLSM image of SH-SY5Y cells incubated for 24 hours with PS/(PLL/PLG)/PLL/iAβ5-FITC/$(PLL/PLG)_3$ nanoparticles. The arrowhead indicates an aggregate of nanoparticles

In figure 3.14, an aggregate of nanoparticles adherent to the cell surface can be seen (indicated by the green fluorescence), while in figure 3.15 only a single nanocapsule is visible in each image (images in the right column, arrowheads). The presence of large aggregates of nanoparticles (figure 3.14) hinders the possibility of cell internalization. In what concerns to nanocapsules (figure 3.15), confocal microscopy shows their effective presence in the medium, since green fluorescence can be seen in the images in the left column, which were obtained while only the green fluorescence channel was

active. Their internalization is also confirmed, since they are in the same focal plane as the cell nucleus, as can be seen in the images in the right column, obtained by the overlapping of all active channels. Apparently, the original morphology of SH-SY5Y cells was not altered by the internalization of the nanocapsules.

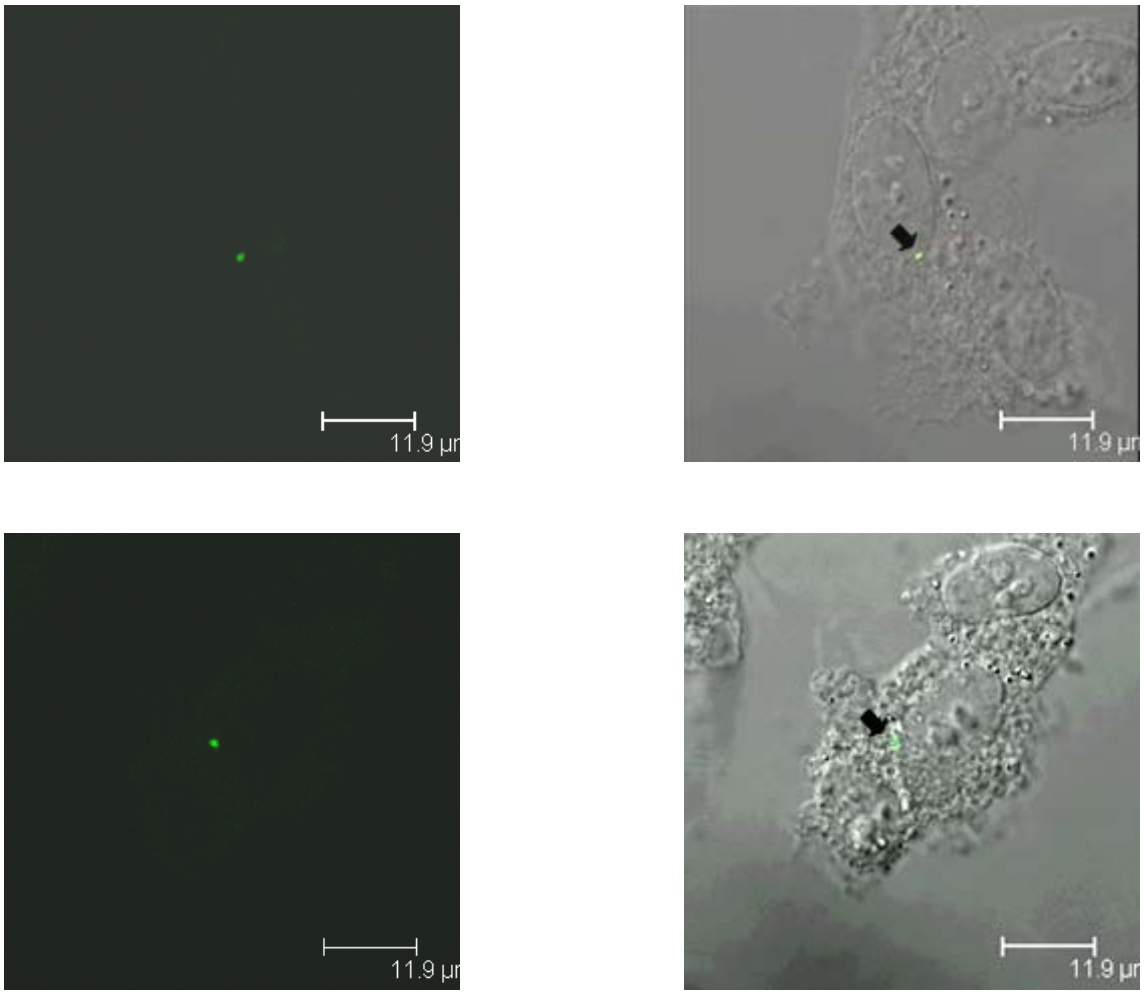

Figure 3.15 – CLSM images of SH-SY5Y cells incubated for 24 hours with PLL/PLG nanocapsules, produced using PS cores with 1 µm of diameter. The outermost layer is PLG, and the second last layer is PLL-FITC. Left column: images captioned with only the green fluorescence channel active. Right column: the correspondent images, obtained by the overlapping of all active channels. The arrowheads indicate a nanocapsule

Wattendorf and colleagues studied cell recognition and phagocytosis of PAH/PSS microcapsules using dendritic cell and macrophage cell cultures obtained from human peripheral blood monocytes (Wattendorf *et al.*, 2008). They found that an additional modification of the surface of the microcapsules with poly(L-lysine)-graft-poly(ethylene

glycol) significantly blocked their phagocytosis by cells, suggesting that strategy as a way of reducing protein adsorption and subsequent phagocytosis of particles upon entering the bloodstream (Wattendorf *et al.*, 2008). Fluorescently labeled hollow polyelectrolyte shells containing five bilayers of gelatine and poly(dimethyldiallyl ammonium chloride) with different outermost layers (PAH, PLL and PSS) were found to be internalized by human breast cancer MCF-7 cells (Ai *et al.*, 2005). LbL microcapsules of anionic dextran sulfate and cationic PLL, produced with $CaCO_3$ templates, were effectively internalized by cultured mice bone-marrow derived dendritic cells (De Koker *et al.*, 2007).

The effects of PSS/PAH microcapsules on viability, proliferation and morphology of 3T3 fibroblast cells cultured in 2D and in a 3D collagen matrix, and of C6 glioma cells cultured in 2D, were studied by An and colleagues (An *et al.*, 2009). Using $MnCO_3$ template particles of several diameters (1-2, 3-6 and 8-10 μm), the authors prepared LbL microcapsules of synthetically and naturally occurring polyelectrolytes, such as PSS/PAH, bovine serum albumin (BSA)/PAH, dextran sulfate/chitosan (CHI) and alginic acid (ALG)/poly(L-lysine) (PLL) microcapsules (An *et al.*, 2009). When microcapsule to cell ratios were ≤ 10:1, PSS/PAH microcapsules did not affect the original morphology of the two types of cells (cultured in 2D monolayers) (An *et al.*, 2009). In fact, glioma cells with internalized PSS/PAH microcapsules kept their normal morphology and intact nuclei (An *et al.*, 2009). The authors also observed that, at a microcapsule to cell ratio of 10:1, no significant differences were found in the uptakes, by C6 cells, of the microcapsules indicated above, despite their different compositions indicated above (An *et al.*, 2009), suggesting that, at that ratio, the biocompatibility of the materials used in the production of microcapsules is not a decisive factor for their successful cellular uptake. On the other hand, increasing the microcapsule concentration

led to a decrease in the number of viable cells of both types (An *et al.*, 2009). In the case of PSS/PAH microcapsules incubated with C6 cells for 24 hours at a microcapsule to cell ratio of 100:1, the loss of cellular viability was attributable to apoptosis (An *et al.*, 2009). With the purpose of studying the hypothetical behavior of PSS/PAH microcapsules in *in vivo* environments, An and colleagues cultured, in collagen gels, C6 glioma cells as multicellular tumor spheroids (MTS), which possess cell-cell and cell-matrix contacts similar to *in vivo* conditions (An *et al.*, 2009). PSS/PAH microcapsules were then placed in the 3D cultures, at the same concentrations employed in the 2D studies, and bright field images were collected (5, 22 and 98 hours after implantation) (An *et al.*, 2009). The results showed that 3D cultures of C6 cells are less affected by the presence of microcapsules than 2D cultures, and also that high concentrations of PSS/PAH microcapsules had no appreciable effect on the growth of MTS (An *et al.*, 2009). Thus, this type of microcapsules is useful as vehicles for delivery of active molecules (An *et al.*, 2009).

Nanosystems carrying active molecules have also been studied in terms of their interaction with cells. The *in vitro* interaction study of chitosan nanoparticles containing FITC-bovine serum albumin, prepared by ionic crosslinking with TPP, with human conjunctival epithelial cells (IOBA-NHC), a cell line derived from normal human conjunctival epithelium showed particle internalization without altering the cell viability (de Salamanca *et al.*, 2006). Chitosan nanocapsules loaded with salmon calcitonin were put in contact with a Caco-2 (enterocyte-like) cell monolayer and with a coculture of Caco-2 and HT29-M6 cells (the latter being mucus-secreting cells) (Prego *et al.*, 2006). Chitosan improves the oral absorption of salmon calcitonin (Prego *et al.*, 2006), so Caco-2 and HT29-M6 cells were chosen as an *in vitro* cell culture model of the small intestine environment. The interaction of CS nanocapsules with Caco-2 cells and their

main interaction with HT29-M6 cells when in coculture was demonstrated by confocal microscopy, which, along with the prolonging of the intestinal absorption of salmon calcitonin, supported their mucoadhesivity (Prego *et al.*, 2006).

The comparison between the results and findings of the various works above and the results obtained in the present work points towards the need of further work in what concerns to the improvement of the stability of both nanoparticles and nanocapsules, in order to avoid aggregation among them. A more effective means of visual delimitation of the cellular membranes should also be employed, for a better clarification of the internalization of the nanosystems.

4 The chitosan/gum arabic system

4.1 Introduction

Polysaccharides are molecules of natural origin (Sinha and Kumria, 2001), being non-toxic, hydrophilic and biodegradable (Liu *et al.*, 2008). Polysaccharides are capable of increasing the absorbance of drugs, when used in the production of nanocarriers (Liu *et al.*, 2008).

Chitosan (CS) is a polysaccharide obtained from the partial alkaline *N*-deacetylation of chitin (Espinoza-Andrews *et al.*, 2007; Hejazi and Amiji, 2003; Illum, 1998). It contains two types of residues, namely 2-acetamido-2-deoxy-β-D-glucopyranose and 2-amino-2-deoxy-β-D-glucopyranose, therefore being a copolymer (Espinoza-Andrews *et al.*, 2007). Figures 4.1 and 4.2 show the chemical structures of chitin and chitosan, respectively. Since *Crustacea* are the most important source of chitin (Hejazi and Amiji, 2003), this polysaccharide is a largely available substance (Liu *et al.*, 2008).

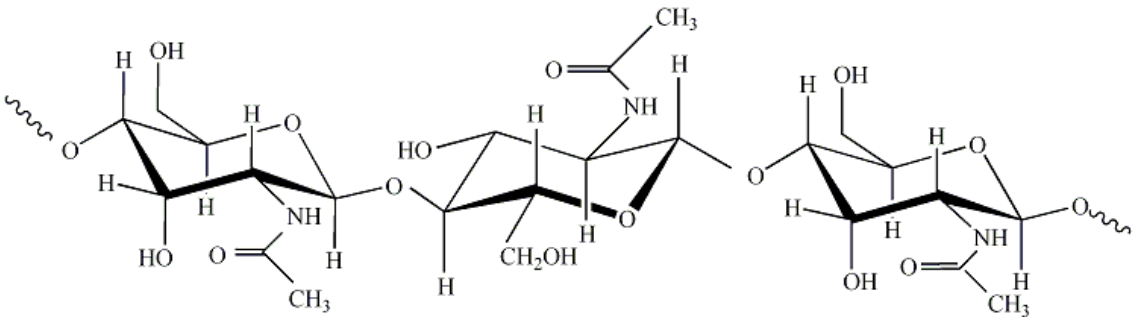

Figure 4.1 – Chemical structure of chitin

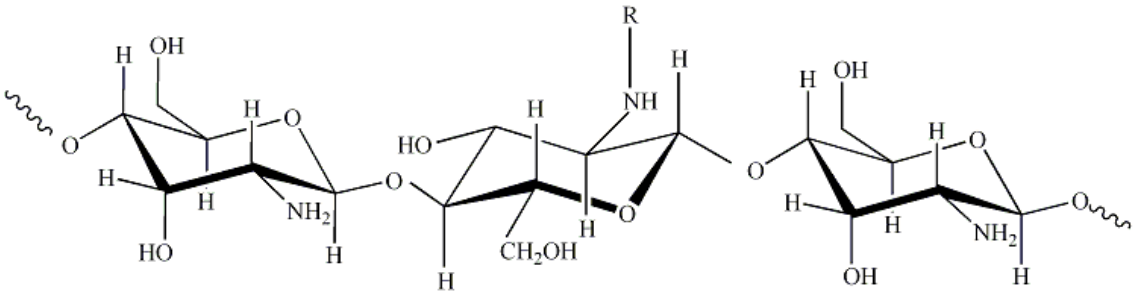

Figure 4.2 – Chemical structure of chitosan. It is composed of 2-amino-2-deoxy-β-D-glucopyranose (R=H) and 2-acetamido-2-deoxy-β-D-glucopyranose ($R=COCH_3$) residues

The degree of *N*-deacetylation and molecular weight of CS may vary largely, normally ranging from 40 to 98%, and from 50,000 to 2,000,000 Da, respectively (Hejazi and Amiji, 2003). Since the pK_a of the 2-amino-2-deoxy-β-D-glucopyranose residue is of 6.2-7.0 (Hejazi and Amiji, 2003), CS is typically insoluble at basic and neutral pH, forming salts with inorganic and organic acids, such as hydrochloric and acetic acid, respectively (Hejazi and Amiji, 2003). Indeed, the protonation of CS amine groups occurs at acidic pH values, making this polysaccharide water–soluble and positively charged under these conditions (Espinoza-Andrews *et al.*, 2007; Hejazi and Amiji, 2003; Illum, 1998), having one positive charge per 2-amino-2-deoxy-β-D-glucopyranose unit (Hejazi and Amiji, 2003). Lower degrees of *N* – deacetylation (≤40%) permit solubilities up to a pH of 9, while the more commonly used CS, with higher degrees of *N*-deacetylation (≥85%), are soluble only up to a pH of 6.5 (Hejazi and Amiji, 2003). The viscosity of CS solutions increases with its concentration and with the decrease of temperature and ionic strength (Espinoza-Andrews *et al.*, 2007; Hejazi and Amiji, 2003). CS with high degree of *N*–deacetylation has flexible chains, due to the high number of positive charges, and therefore it adopts an extended conformation, whereas CS with lower degree of *N*–deacetylation, with a lower number of positive charges, adopts a more coiled conformation. Consequently, there is a relationship between the degree of N-deacetylation of CS and the viscosity of the

respective solutions (Illum, 1998). Another characteristic of CS is its mucoadhesiveness, due to the capability of its positively charged amino groups to interact with negatively charged sialic acid residues of mucus (de Campos *et al.*, 2004).

CS nanoparticles are generally produced through rapid processes, which involve only mild conditions. Being a positively-charged polymer under acidic pH values, CS can be combined with anionic polymers, producing CS nanoparticles through the spontaneous formation of CS/polyanion complexes (Reis *et al.*, 2006a). Moreover, combining CS with oppositely charged polymers may neutralize its positive charge and consequently reduce its cytotoxicity (Chen *et al.*, 2007).

One of the most widely used methods in the production of CS nanoparticles is the ionotropic gelation of CS with pentasodium tripolyphosphate (TPP), a polyanion (Calvo *et al.*, 1997) (figure 4.3). This method is also referred to as ionic crosslinking (Liu *et al.*, 2008).

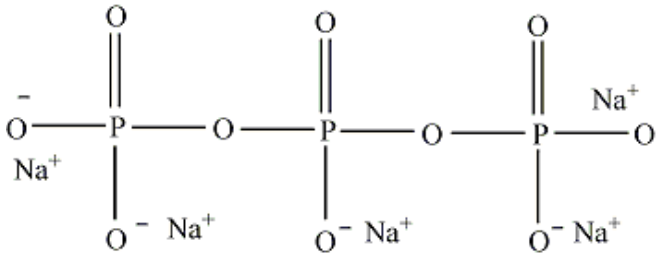

Figure 4.3 – Chemical structure of TPP

Intra- and intermolecular ionic interactions are established between the positively charged amine groups of CS and the negatively charged groups of TPP (Calvo *et al.*, 1997).

Due to all the advantageous characteristics aforementioned, CS can be seen as an ideal hydrophilic carrier system (Aktas *et al.*, 2005). Indeed, food additives, biomedicine and pharmaceuticals are some of the areas where CS can be used (Hajdu *et al.*, 2008). The favourable properties of CS nanoparticles, in what concerns to the incorporation of

bioactive compounds (de Campos *et al.*, 2004) and the promotion of their absorption through mucous surfaces (Illum, 1998; Pan *et al.*, 2002), can be improved through the combination of CS with other components, producing complex nanoparticles (Xu and Du, 2003). Polyelectrolyte complexation (PEC) is the process by which oppositely charged polymers spontaneously interact with each other, by means of electrostatic intermolecular forces (Liu *et al.*, 2008). For example, CS has been combined with negatively charged polymers such as alginate (Sarmento *et al.*, 2006) and dextran sulfate (Chen *et al.*, 2007; Sarmento *et al.*, 2006).

Gum arabic (GA) is a mixture of polysaccharides and glycoproteins with various compositions and molecular weights (Espinoza-Andrews *et al.*, 2007). It possesses a main galactan chain, from which numerous polysaccharide side chains emerge, conferring it an overall branched polymer structure. It is mainly composed of D-galactose (~40%) and L-arabinose (~24%), as well as uronic acids such as D-glucuronic acid (~21%) and 4-*O*-methyl-D-glucuronic acid (~2%) (Espinoza-Andrews *et al.*, 2007). Figure 4.4 (a) – c)) shows the Haworth projections of the main components of GA.

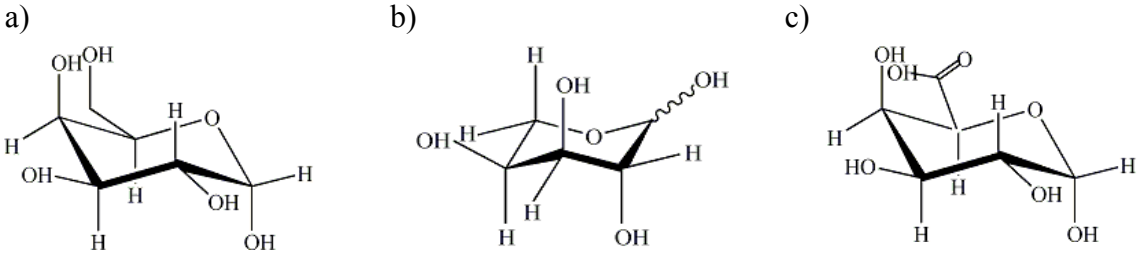

Figure 4.4 – Haworth projections of the main components of GA: a) D-galactose; b) L-arabinose and c) D-glucuronic acid.

Due to the amount of uronic acids present in GA (Espinoza-Andrews *et al.*, 2007), GA was chosen as a polyanion donor, for the polyelectrolyte complexation with CS. Moreover, GA is an effective encapsulating agent, highly water-soluble, with emulsifying properties, and capable of producing low-viscosity concentrated solutions

(Mcnamee *et al.*, 1998). Thus, a polymeric carrier system consisting on the combination of two compounds described in the literature as good encapsulating agents, namely CS and GA, might be extremely advantageous for drug delivery.

4.2 Polymers used

Chitosan, having a high molecular weight (~325,000) and a degree of deacetylation of 75.6%, and Gum Arabic, with a molecular weight of ~250,000, were purchased from Sigma.

4.3 Preparation of CS:GA nanoparticles

CS:GA nanoparticles were prepared by polyelectrolyte complexation.

Solutions of CS in acetic acid 1% were prepared at concentrations of 0.60 mg/mL and 3.0 mg/mL. The suitable masses of CS were dissolved in 5 mL of acetic acid 1% solution, followed by pH adjustment to a value between 4.7 and 4.9 with NaOH 10% solution. GA aqueous solutions were prepared by dissolving the suitable GA masses in 5 mL of ultrapure water.

The following CS:GA charge ratios were prepared: 1:0.03; 1:0.09; 1:0.25; 1:0.3; 1:0.34; 1:0.6; 1:1; 1:1.25; 1:1.4 and 1:1.7. The nanoparticles' suspensions were prepared by adding 5 mL of the correspondent GA solution to 5 mL of a CS solution, dropwise, under magnetic stirring, at room temperature. After the addition of GA, the samples were left under magnetic stirring for sixty minutes.

The number of positive charges per millilitre of CS solution was estimated taking into account the average molecular weight (325,000) and degree of deacetylation (75.6%) of

CS. It was also assumed that, at the pH conditions used, there was one positive charge per each 2-amino-2-deoxy-β-D-glucopyranose residue in solution. The number of negative charges per millilitre of each GA solution was estimated assuming that the only charged residues of GA are D-glucuronic acid and 4-*O*-methyl-D-glucuronic acid, each residue having one negative charge. Their relative amounts in a GA molecule were assumed to be 21% (D-glucuronic acid) and 2% (4-*O*-methyl-D-glucuronic acid) (Espinoza-Andrews *et al.*, 2007).

4.3.1 Turbidity measurements

The results of the turbidity measurements of CS:GA nanoparticles' suspensions are depicted in figure 4.5.

The turbidity of the nanoparticles' suspensions increases as the number of added negative charges increases, until visible aggregation occurs for a given CS:GA charge ratio (data not shown). This phenomenon was observed for CS:GA 1:1.25, 1:1.4 and 1:1.7 at a CS initial concentration of 0.60 mg/mL, and for CS:GA 1:1, 1:1.25, 1:1.4 and 1:1.7 at a CS initial concentration of 3.0 mg/mL.

In previous studies, Schatz and colleagues studied the polyelectrolyte complexation of CS (polycation donor) and dextran sulfate (DS) (polyanion donor) (Schatz *et al.*, 2004a; Schatz *et al.*, 2004b). The authors prepared the polyelectrolyte solutions under experimental conditions very similar to those followed in this work (Schatz *et al.*, 2004a; Schatz *et al.*, 2004b).

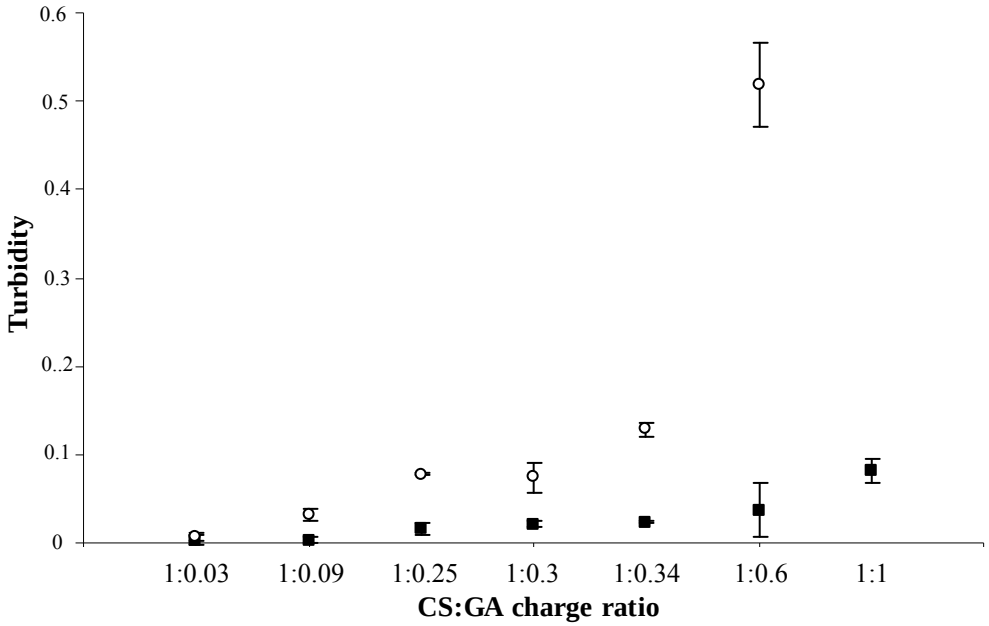

Figure 4.5 – Turbidity of nanoparticles' suspensions of various CS:GA charge ratios, produced using an initial CS concentration of 0.60 mg/mL (■) and 3.0 mg/mL (○) (Mean ± S.D.; *N*=3)

The DS solutions were added dropwise to the CS solutions, at different charge ratios between cationic and anionic charged units (n^+/n^-), and the turbidity of the resulting complex dispersions was measured at a wavelength of 500 nm (Schatz *et al.*, 2004a; Schatz *et al.*, 2004b). It was observed that, regardless of the molecular weight of CS and DS used, there was an increase of turbidity as the concentration of negative charges increased, indicating the formation of increasing amounts of insoluble polyelectrolyte complexes, until the n^+/n^- of 1 was reached, where flocculation occurred (Schatz *et al.*, 2004a; Schatz *et al.*, 2004b). Up to that n^+/n^-, the presence of free unpaired positive charges at the surface of the nanoparticles assured their electrostatic stabilization. At the n^+/n^- of 1, there was full charge neutralization, and hence the nanoparticles became uncharged, which led to their aggregation (Schatz *et al.*, 2004a; Schatz *et al.*, 2004b). In a study concerning the formation of polyelectrolyte complexes between CS and poly-γ-glutamic acid (PGA) (polycation and polyanion donors, respectively), the precipitation of the obtained nanosystems, for a given CS:PGA mass proportion, was also justified by

the lack of availability of free charged amino groups at their surface (Hajdu *et al.*, 2008). The results shown in figure 4.5 can be explained taking into account the works described above. Indeed, the increase in turbidity of the CS:GA nanoparticles' suspensions, as a function of the CS:GA charge ratio, indicates that increasingly higher numbers of negative charges, put in contact with the initial CS solutions, lead to the production of increasingly higher amounts of nanoparticles. The visible aggregation obtained for CS:GA charge ratios of around 1:1 can be explained by the full compensation of the positive charges of CS by the negative charges of GA, which leads to the obtention of uncharged nanoparticles, that aggregate and precipitate.

The turbidity values of solutions produced using a CS initial concentration of 3.0 mg/mL (figure 4.5, ○ curve) are significantly higher than those produced using a CS initial concentration of 0.60 mg/mL (figure 4.5, ■ curve). In a previous study, Alonso-Sande and colleagues focused on the formation of nanoparticles, made of CS and phosphorylated glucomannan (GM) (polyanion donor), by electrostatic interactions (Alonso-Sande *et al.*, 2006). The CS and GM polyelectrolyte solutions were prepared under experimental conditions very similar to those followed in this work. Indeed, CS was dissolved in acetic acid 1% solution to a concentration of 2 mg/mL, followed by the raising of the pH to 4.8 with NaOH 10 *M* solution. The GM solution was prepared through the dissolution of GM in ultrapure water, to a concentration of 23 mg/mL (Alonso-Sande *et al.*, 2006). CS:GM nanoparticles were formed by the incorporation of prefixed volumes of GM solution onto 3 mL of the CS solution. Two CS:GM mass proportions were studied, namely 1:0.77 and 1:2.3 (Alonso-Sande *et al.*, 2006). The authors found that an increase in the amount of the polyanion donor (GM) led to the formation of a greater number of nanoparticles, *i.e.* the CS:GM mass proportion of 1:2.3 produced a greater number of nanoparticles, when compared to the proportion of 1:0.77

(Alonso-Sande *et al.*, 2006). Their explanation for these results relied on the fact that a higher amount of negatively charged GM molecules meant a higher ionic strength in the medium, which in turn may improve the interaction between the two polymers (Alonso-Sande *et al.*, 2006). Taking into account these previous results, the higher turbidity values found for nanoparticles' suspensions produced with a CS initial concentration of 3.0 mg/mL, when compared to a CS initial concentration of 0.60 mg/mL (figure 4.5), may be due to the fact that, in the first case, the ionic strength of the medium is higher, thus improving the interaction of CS and GA. Even though in the present work ionic strength was not controlled, one can assume that increasing the concentration of the polymeric solutions implies a higher ionic strength. Indeed, figure 4.5 shows that, for each CS:GA charge ratio, higher turbidity values (therefore, a greater number of nanoparticles), were always obtained when CS initial concentration was 3.0 mg/mL. Also, the fact that, when CS initial concentration was 3.0 mg/mL, visible aggregation occurred for a lower number of negative charges in the medium (CS:GA 1:1), when compared to when CS initial concentration was 0.60 mg/mL (CS:GA 1:1.25), might be equally explained by the higher ionic force of the medium in the first case, which led to a greater interaction between the two polymers. This might have induced the full compensation of the positive charges of CS by the negative charges of GA, with subsequent aggregation of the resulting neutral nanoparticles, at a lower CS:GA charge ratio.

4.3.2 Determination of process yield

The nanoparticles' production yields were calculated following a procedure adapted from the literature (Alonso-Sande *et al.*, 2006). Briefly, the nanoparticles' suspensions

were centrifuged at 20000 *g*, for 60 min, at 6 ºC. The supernatants were rejected, and the sediments were resuspended in 1 mL of acetic acid 1% solution, using stirring and ultrasounds, followed by freeze-drying for 24 h. The theoretical solids' weights were estimated and the real weight of freeze-dried nanoparticles was measured.

Two sets of three independent CS:GA nanoparticles' suspensions (volume of each suspension = 5 mL) were used, both at an initial CS concentration of 0.60 mg/mL and 3.0 mg/mL. Both sets had a CS:GA charge ratio of 1:0.34. The following relation leads to the determination of the process yield:

$$\text{process yield (\%)} = \frac{\text{nanoparticles weight}}{\text{total solids (CS + GA) weight}} \times 100 \qquad (4.1)$$

The process yield for a CS initial concentration of 0.60 mg/mL was 56 ± 14%, while a process yield of 61 ± 3% was obtained for a CS initial concentration of 3.0 mg/mL. These results suggest that there was no significant difference between the process yield of the two CS initial concentrations studied.

4.4 Characterization of CS:GA nanoparticles

4.4.1 Size distribution and stability of the nanoparticles

The formation of nanoparticles was followed by dynamic light scattering (DLS) and zeta potential (ZP) measurements.

Hydrodynamic diameters of triplicates of each different CS:GA charge ratio (diluted 1:50 in ultrapure water), at both CS initial concentrations, 0.60 mg/mL and 3.0 mg/mL, are presented in figures 4.6 and 4.7, respectively. Aggregates, rather than a homogenous

nanoparticles suspension, were obtained for CS:GA charge ratios of 1:1.25, 1:1.4 and 1:1.7, at a CS initial concentration of 0.60 mg/mL (figure 4.6) (data not shown). For a higher CS initial concentration (3.0 mg/mL) (figure 4.7), the onset of aggregation occurs already at a CS:GA charge ratio of 1:1 (data not shown).

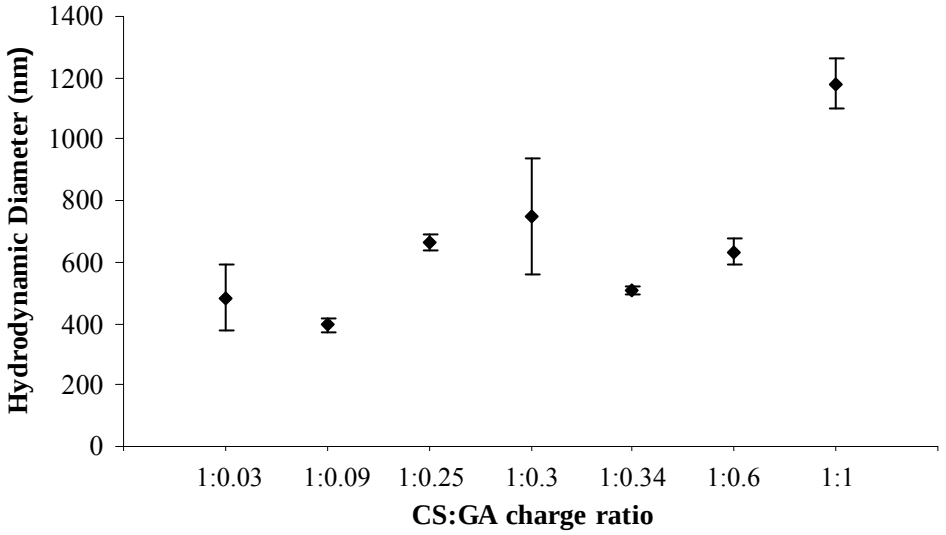

Figure 4.6 – Hydrodynamic diameters of nanoparticles' suspensions of various CS:GA charge ratios, produced using an initial CS concentration of 0.60 mg/mL (for each CS:GA charge ratio, Mean ± S.D. is depicted, and *N*=3)

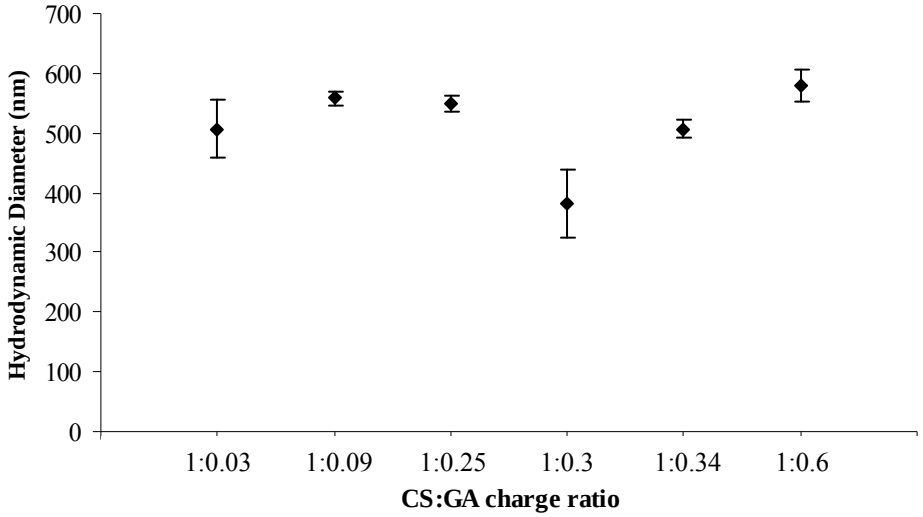

Figure 4.7 – Hydrodynamic diameters of nanoparticles' suspensions of various CS:GA charge ratios, produced using an initial CS concentration of 3.0 mg/mL (for each CS:GA charge ratio, Mean ± S.D. is depicted, and *N*=3)

ZP measurements of each nanoparticles' suspension (diluted 1:50 in ultrapure water) were also performed. Figures 4.8 and 4.9 present the ZP values of triplicates for each CS:GA charge ratio, at the CS initial concentrations of 0.60 mg/mL and 3.0 mg/mL, respectively.

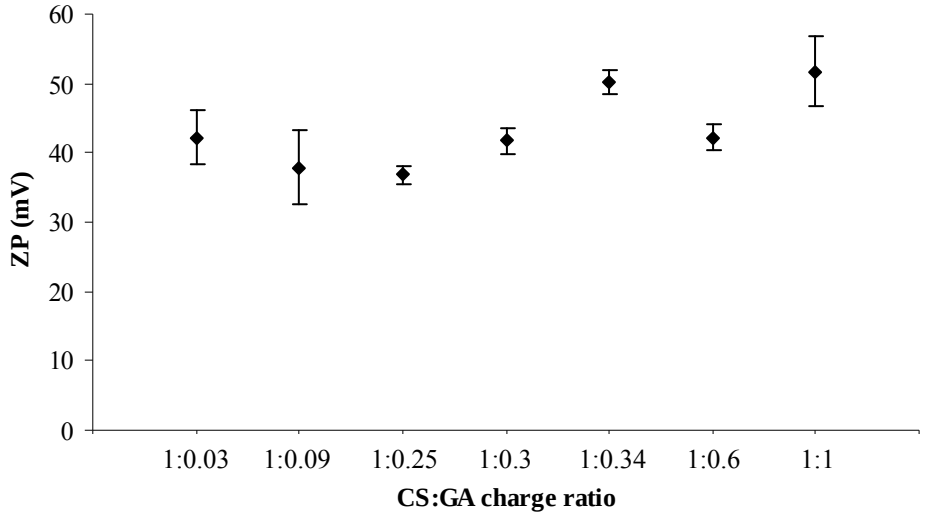

Figure 4.8 – Zeta potential of nanoparticles' suspensions of various CS:GA charge ratios, produced using an initial CS concentration of 0.60 mg/mL (for each CS:GA charge ratio, Mean ± S.D. is depicted, and *N*=3)

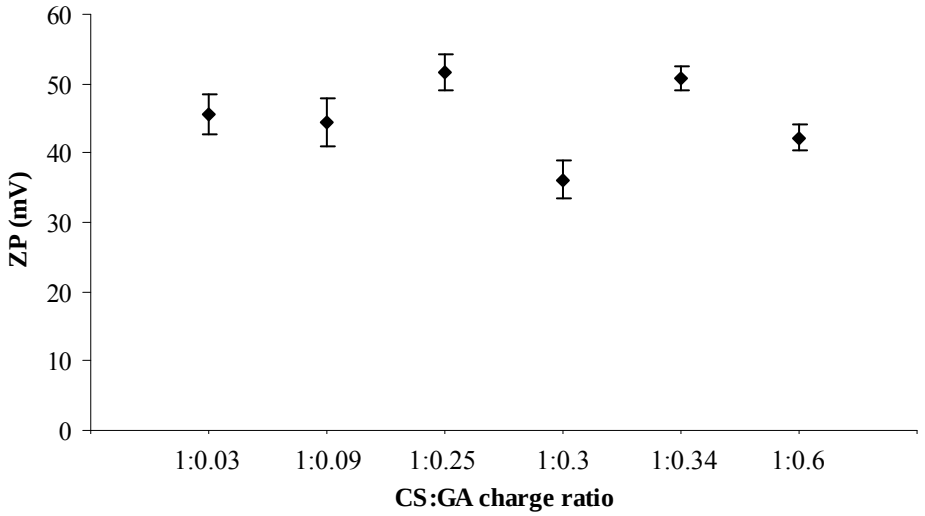

Figure 4.9 – Zeta potential of nanoparticles' suspensions of various CS:GA charge ratios, produced using an initial CS concentration of 3.0 mg/mL (for each CS:GA charge ratio, Mean ± S.D. is depicted, and *N*=3)

The observed differences in the CS:GA charge ratio at which the onset of visible aggregation occurs, depending on CS initial concentration, are in agreement with those obtained for turbidity measurements (section 4.3.1, figure 4.5). The respective interpretation can again rely on the differences of ionic strength of the medium, in the light of the work of Alonso-Sande and colleagues (Alonso-Sande *et al.*, 2006), and is similar to the one made for turbidity measurements (section 4.3.1).

In what concerns to the variation of the hydrodynamic diameter of the nanoparticles as a function of CS:GA charge ratio, the analysis of figures 4.6 and 4.7 shows that, independently of the CS initial concentration used, there is not a significant variation of their hydrodynamic diameter as the number of negative charges increases. Until aggregation occurred, the nanoparticles displayed hydrodynamic diameters that ranged between 400 – 600 nm, except at charge ratio of 1:1 at a CS initial concentration of 0.60 mg/mL that reached diameters of 1200 nm and eventually precipitate. The variation of ZP of the nanoparticles as a function of CS:GA charge ratio is shown in figures 4.8 and 4.9, where it can be seen that, regardless of the CS initial concentration used, there is not a significant variation of ZP as the number of negative charges in the medium increases. Until aggregation occurred, the nanoparticles displayed ZP values that ranged between 30 to 55 mV.

In a study concerning the polyelectrolyte complexation of CS (polycation donor) and dextran sulfate (DS) (polyanion donor), Schatz and colleagues used two different chitosans and three different dextran sulfates. One CS had a low molecular weight (~16,000) and the other had a high molecular weight (~365,000). Both had a degree of deacetylation of 85%. The DS had a molecular weight of 5,000; 10,000 and 1,510,000, respectively, all of them possessing a degree of sulfation of 2.2 – 2.4 (Schatz *et al.*, 2004a). The several polyelectrolyte solutions were prepared under experimental

conditions similar to those followed in the present work, namely in what concerns to the dissolution of CS in acidic solutions and the dissolution of DS in deionized water (Schatz *et al.*, 2004a). The pH (pH 4.0) and ionic strength of both solutions were adjusted and controlled (Schatz *et al.*, 2004a). Using chitosan as the starting solution, the formation of polyelectrolyte complexes was carried on at room temperature, DS solutions being added dropwise to CS solutions. This was performed for charge ratios between cationic and anionic charged units (n^+/n^-) higher than 1 (implying a number of cationic charges in the medium always higher than that of anionic charges) (Schatz *et al.*, 2004a). DLS and turbidity measurements showed that nanoparticles' hydrodynamic diameters and turbidity values where higher for high molecular weight CS, when compared to low molecular weight CS. On the other hand, an increase in DS molecular weight led to lower hydrodynamic diameters and turbidity values. In all cases, nanoparticles' hydrodynamic diameters decreased during the addition of the DS solutions to the CS starting solutions, until aggregation and flocculation occurred (Schatz *et al.*, 2004a). Based on these observations, the authors considered that the formation of nanoparticles involved the successive segregation of segments, formed on polymer chains due to charge neutralization, to the core of the nanoparticles. Free unpaired charges are placed in the corona of the nanoparticles, stabilizing them (Schatz *et al.*, 2004a). Thus, the higher the chain length of CS (*i.e.*, its molecular weight), the thicker the nanoparticles' corona, and the greater their hydrodynamic diameter. On the other hand, the greater the extension of polymeric sections where charge neutralization has occurred, the smaller the nanoparticles (Schatz *et al.*, 2004a). Indeed, the gradual addition of DS solutions to the CS starting solutions implied a gradual reduction in the hydrodynamic diameters of the nanoparticles, because the positive charges of CS chains present in their corona were gradually neutralized by the negative charges of DS chains,

and the resulting segments collapsed onto the core of the nanoparticles (Schatz *et al.*, 2004a). The authors also stated that the relationship between the molecular weights of CS and DS played an important role in the formation, surface charge and stability of nanoparticles. When a low molecular weight DS is mixed with a high molecular weight CS, in the presence of an excess of CS (positive charges), CS chains can act as host polycation. The uncharged segments formed by the local neutralization of positive charges will be segregated to the core of the nanoparticles, while there will still be a sufficient number of free positive charges at their surface for their stabilization to be possible. If a high molecular weight DS is mixed with a low molecular weight CS, it is the polyanion (DS) that will act as a host. The uncharged segments formed by the local neutralization of negative charges will be longer than in the previous case (because there is an excess of CS), and more compact nanoparticles will be produced. The excess of CS also allows their stabilization, since there will be free positive charges at their surface. When in the presence of an excess of DS (negative charges), a low molecular weight DS is mixed with a high molecular weight CS, the small DS molecules completely neutralize the positive charges along CS chains, and the resulting nanoparticles do not possess enough free charges at their surface, capable of stabilizing them, and thus they aggregate. On the contrary, if an excess of high molecular weight DS is mixed with a low molecular weight CS, the local neutralization of negative charges leads to the formation of uncharged segments, which will form the core of the nanoparticles, while the non-neutralized, free negative charges in some segments of DS chains will constitute their corona, stabilizing them. In all cases mentioned, when n^+/n^- reached 1, irreversible flocculation of the nanoparticles' suspensions occurred (Schatz *et al.*, 2004a).

The CS and GA molecules used in the present work have molecular weights of the same order of magnitude, namely ~325,000 for CS and ~250,000 for GA. Hence, it is not predictable that the complexation between the two polymers relied on "host-guest" interactions. Nevertheless, while in the work of Schatz and colleagues each DS molecule was more charged than each CS molecule (Schatz *et al.*, 2004a), in the present work it is the CS molecules that are more charged than the GA molecules. Indeed, each CS molecule was estimated to have 1299 positive charges, based on the molecular weight of CS, its degree of deacetylation (75.6%), and assuming that, under the experimental conditions followed, there was one positive charge per each 2-amino-2-deoxy-β-D-glucopyranose residue. In what concerns to GA, each molecule was estimated to have 294 negative charges, based on the molecular weight of GA, and taking into account the work of Espinoza-Andrews and colleagues, who stated that the only charged residues of GA are D-glucuronic acid and 4-*O*-methyl-D-glucuronic acid, each residue having one negative charge. Their relative amounts in a GA molecule were assumed to be 21% (D-glucuronic acid) and 2% (4-*O*-methyl-D-glucuronic acid) (Espinoza-Andrews *et al.*, 2007).

Thus, the results presented in figures 4.6 – 4.9 can be interpreted in the light of the conclusions of Schatz and colleagues mentioned above, taking into consideration the particular characteristics of the polymers used in the present work. Up to CS:GA charge ratio of 1:1, the number of positive charges in the medium is higher than that of negative charges. Consequently, the core of the nanoparticles is composed of the segregated segments resulting from the local neutralization of positive charges of CS, while at the same time the remaining free, non-neutralized positive charges are located at the surface of the nanoparticles, stabilizing them. Indeed, until aggregation occurs, positive ZP values are always displayed, regardless of the CS:GA charge ratio (figures

4.8 and 4.9). Moreover, given the fact that only 23% of GA residues are charged, GA chains possess large non-charged segments. Consequently, one can speculate that the core of the CS:GA nanoparticles is in fact composed as well of the referred hydrophobic segments of GA. As a consequence, contrary to the observations of Schatz and colleagues relative to the CS:DS system (Schatz *et al.*, 2004a), in the case of the CS:GA system, the nanoparticles' size reduction as a result of the consumption of superficial positive charges and subsequent collapse of the uncharged segments onto their hydrophobic core results not detectable, due to the presence of large uncharged segments in the nanoparticles' cores. The lack of significant variation of the nanoparticles' hydrodynamic diameters, despite the increase in the number of negative charges in the medium, presented in figures 4.6 and 4.7, supports this interpretation.

4.4.2 Morphology of the nanoparticles

Figures 4.10 and 4.11 show transmission electron microscopy (TEM) micrographs of CS:GA 1:0.3 nanoparticles (using a CS initial concentration of 3.0 mg/mL).

The nanoparticles have an overall spherical shape, with a certain degree of size polydispersion. Indeed, their size appears to range from 50 to nearly 200 nm. This size range is lower than the one indicated by DLS measurements (section 4.4.1, figure 4.7). Again, this phenomenon might be explained taking into account the work of Aktas and colleagues, who stated that the high swelling capacity of CS nanoparticles in wet mediums was the reason underlining the discrepancies between their hydrodynamic diameter, measured by DLS, and their size estimated by TEM (Aktas *et al.*, 2005). The same assumptions were made by Chen and colleagues, concerning similar results

obtained for CS:DS nanoparticles (Chen *et al.*, 2007), and by Hajdu and colleagues, regarding CS:PGA nanoparticles (Hajdu *et al.*, 2008).

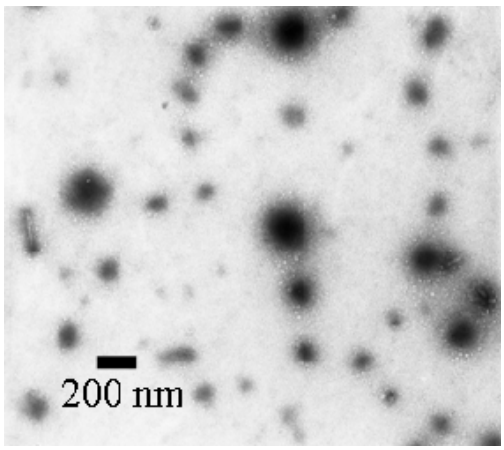

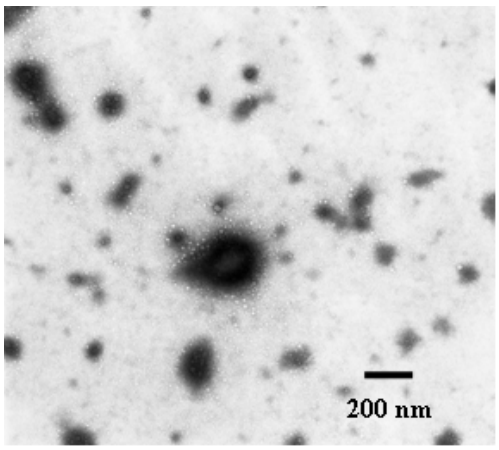

Figures 4.10 and 4.11 – TEM micrographs of CS:GA 1:0.3 nanoparticles (CS initial concentration of 3.0 mg/mL)

In figure 4.12 (a) – c)), atomic force microscopy (AFM) micrographs of CS:GA 1:0.34 nanoparticles (using a CS initial concentration of 0.60 mg/mL) are presented. AFM micrographs of CS:GA 1:0.3 nanoparticles (using a CS initial concentration of 3.0 mg/mL) is shown in figure 4.13 (a) and b)). The relatively smooth surface of the nanoparticles, possessing an overall size polydispersion, can be highlighted as a common feature presented in all the AFM images, in agreement with the TEM results. Also, it is of note the presence of vesicular structures, as well as particulate complexes. The formation of vesicular structures as a result of electrostatic interactions between macromolecules is a rare event (Sanchez *et al.*, 2002). In a study focusing on the complex coacervation of β-lactoglobulin (BLG) and GA, Sanchez and colleagues combined the two molecules at several weight ratios (Sanchez *et al.*, 2002). The authors found that, when the less charged polymer (*i.e.*, BLG) was combined with GA (the more charged one) at a BLG:GA weight ratio of 2:1, implying a weight excess of the less charged polymer, multivesicular coacervates were formed by the coalescence of vesicular coacervates (Sanchez *et al.*, 2002).

a)

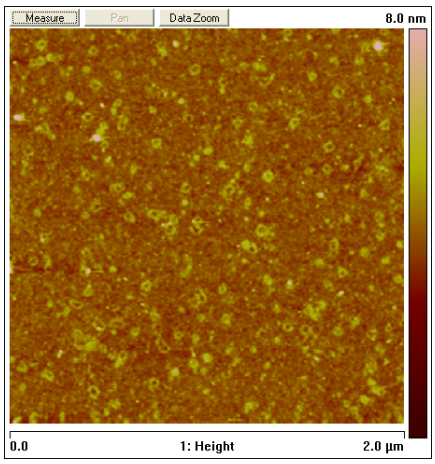

b)

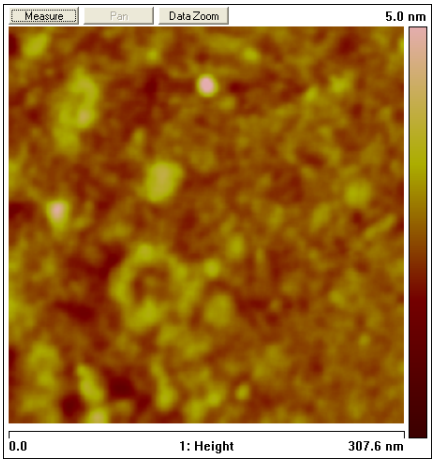

c)

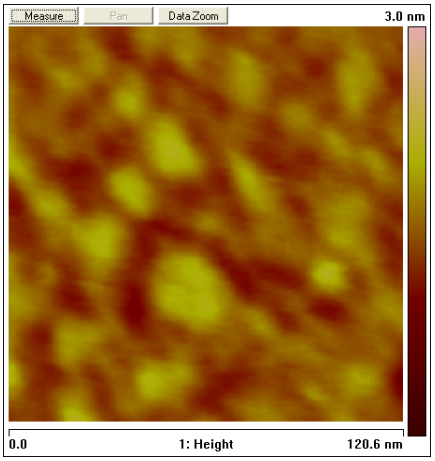

Figure 4.12 – AFM micrographs of CS:GA 1:0.34 nanoparticles (CS initial concentration of 0.60 mg/mL). From a) to c), there is an increase in the magnification used. In all cases, the height of the AFM images is represented by vertical graded brown-light pink scales, on the right side of the respective micrograph

In a study regarding the same polymeric system, Schmitt and colleagues obtained, for the BLG:GA weight ratio of 2:1, vacuolised coacervates, whose formation was also attributed to the partial coalescence of smaller vesicular coacervates (Schmitt *et al.*, 2001).

a) b)

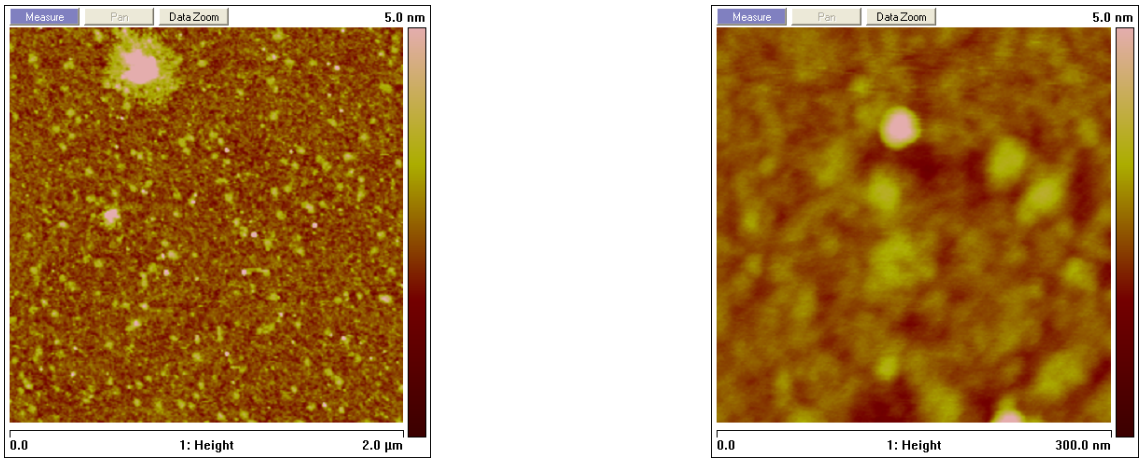

Figure 4.13 – AFM micrographs of CS:GA 1:0.3 nanoparticles (CS initial concentration of 3.0 mg/mL). From a) to b), there is an increase in the magnification used. In both cases, the height of the AFM images is represented by vertical graded brown-light pink scales, on the right side of the respective micrograph

Wolfert and colleagues, studying the interactions between DNA and cationic polymers, found that the use of cationic polymers with a high charge density favoured the formation of more compact DNA/cationic polymer complexes, while supramolecular, vesicle-like structures were obtained when cationic polymers with a low charge density were used (Wolfert *et al.*, 1999). Sanchez and colleagues also stated that the existence of insufficiently neutralized macromolecular complexes seem to favour the formation of vesicles (Sanchez *et al.*, 2002). Taking this into account, and also in the light of the works previously mentioned, the formation of vesicular structures at CS:GA charge ratios of 1:0.3 and 1:0.34 (figures 4.12 and 4.13), both implying a higher number of positive charges, might be attributable to the lack of charge neutralization of the positive charges of CS by the negative charges of GA.

Further comparison of AFM images shows that the vesicular structures are more abundant when a CS initial concentration of 0.60 mg/mL was used (figure 4.12), than when a CS initial concentration of 3.0 mg/mL was used (figure 4.13). In a study on the complex coacervation between CS and GA, Espinoza-Andrews and colleagues explained the higher coacervate yields obtained for high biopolymers´ concentrations in

terms of the higher flexibility of the macromolecular backbones under those conditions, which made the charged sites of the polymers more available for interacting with the oppositely charged sites (Espinoza-Andrews *et al.*, 2007). On the other hand, for lower biopolymers´ concentrations, the polymers expand, leading to gradually more rigid macromolecular backbones, whose charged sites will have lower freedom for interaction (Espinoza-Andrews *et al.*, 2007). Taking into account these findings, one can speculate that, at a CS initial concentration of 0.60 mg/mL (figure 4.12), the formation of particulate complexes was less favoured than at a higher CS initial concentration of 3.0 mg/mL (figure 4.13), which implied a higher overall biopolymer concentration and higher flexibility.

5 Conclusions

Nanospheres and nanocapsules are submicrometer-sized devices, classified under the general name of nanoparticles. Several methods and polymers can be used in their preparation. Polyelectrolytes based on polypeptides are proposed for the preparation of multilayered nanocapsules as they are biodegradable and allow tuning the system stability. Due to their lack of toxicity, their hydrophilicity, bioadhesivity and biodegradability, polysaccharides such as chitosan, alginate and dextran sulfate are regarded as very advantageous polymers for the preparation of nanoparticles. Nanosystems produced with these materials are potentially suitable for administering therapeutic molecules, because they have a subcellular size, biocompatibility with tissues and cells and may have sustained-release and targeting properties.

As therapeutic molecules, peptides and proteins generally have low bioavailability and short half-life in the bloodstream, as well as reduced capacity of crossing biological barriers. iAβ5 is a pentapeptide capable of *in vitro* inhibition of the conformational changes of Amyloid-β peptide, which are responsible for the formation of the amyloid plaques in Alzheimer's disease. In this thesis, two polymeric systems, potentially suitable for the delivery of therapeutic molecules such as iAβ5, have been studied in terms of their physicochemical and morphological features.

Poly(L-lysine)/poly(L-glutamic acid) particles and capsules, either possessing a iAβ5-FITC or a fluorescently-labeled polymeric layer, were produced by the layer-by-layer technique. The successive addition of the several layers was followed by zeta potential measurements, which showed the successful deposition of the oppositely charged polymers. Confocal laser scanning microscopy imaging was used to gain knowledge of the integrity of the polymeric walls of the nanosystems, which were found to possess an

average spherical shape and diameters of around 1 μm. It was found that an increase in the concentration at which the PLL-FITC layer was added enhanced the degree of aggregation of FITC-labeled nanoparticles, a phenomenon potentially attributable to the aggregation of FITC molecules at their surface, given the fact that PLL chains are capable of diffusing "out" of the film. The combined analysis of zeta potential measurements and confocal microscopy images regarding nanoparticles with entrapped iAβ5-FITC within their polymeric layers showed the efficient adsorption of this peptide both to positively and negatively charged layers. These observations might again be explained by the capability of PLL and PLG chains to diffuse when on polyelectrolyte multilayer films. PLL/PLG nanoparticles with entrapped iAβ5-FITC were exposed to acidic and alkaline pH values, in order to study the effects of pH shifts on the integrity of their polymeric layers. Confocal microscopy imaging suggested that, despite the alteration of the pH values to 3 and 10, iAβ5-FITC remained entrapped within the polymeric layers. Although there is a possibility that a certain erosion of the outermost polymeric layers of the nanoparticles occurred, the maintenance of iAβ5-FITC entrapped might be due to the fact that the pH shifts were not extreme and thus were not capable of inducing the film structural reorganizations (β-sheet to α-helix) that are known to cause mass loss and decrease in the thickness of polyelectrolyte multilayer films. Nevertheless, it was found that the alteration of pH to values of 3 and 10 caused aggregation of the nanoparticles. Nanocapsules, obtained by the dissolution of polystyrene cores, were observed by confocal microscopy, which showed the maintenance of the integrity of their walls, their tendentiously spherical shape and their original diameter (~1 μm), despite the high degree of aggregation among them.

More detailed information about the morphology of PLL/PLG nanoparticles and nanocapsules was obtained by transmission electron microscopy and atomic force

microscopy imaging. TEM revealed their spherical shape, the overall integrity of their walls, and showed their tendency to shrink when submitted to drying, a phenomenon particularly of note for nanocapsules. Atomic force microscopy showed the smooth surface of the nanosystems. Taken together, the studies regarding the characterization of PLL/PLG nanoparticles and nanocapsules suggested that the entrapment of iAβ5-FITC within the polymeric layers of nanoparticles is a more valuable strategy of protecting the peptide than its encapsulation in nanocapsules. Besides, nanoparticles were found to be stable at different pH, while nanocapsules presented aggregation problems.

In order to assess the cellular uptake and cytotoxicity of these nanosystems, their interaction with neuroblastoma cells was carried out in *in vitro* studies. The SH-SY5Y cell line (a model cell system for studying neuronal cell death) was incubated with PLL/PLG nanoparticles (containing iAβ5-FITC entrapped) and nanocapsules (having a FITC-labeled polymeric layer). Confocal microscopy imaging confirmed the cellular internalization of nanoparticles, as well as the maintenance of the original cellular morphology. Nevertheless, further improvements of the stability of the nanosystems, as well as the optimization of incubation times and cell staining are required, for a better assessment of the interactions between the cells and the nanosystems.

In what concerns to the chitosan/gum arabic system, nanoparticles were produced at several CS:GA charge ratios, by polyelectrolyte complexation. Turbidity measurements showed an overall tendency of the turbidity of the suspensions to increase with the increase of the number of negative charges, until a given CS:GA charge ratio was reached (CS:GA 1:1.25 for a CS initial concentration of 0.60 mg/mL; CS:GA 1:1 for a CS initial concentration of 3.0 mg/mL), at which visible aggregation was obtained. The increase in turbidity values as a function of the CS:GA charge ratio suggests that the increase of the number of negative charges in the medium caused the production of

gradually higher amounts of nanoparticles. The occurrence of aggregation was due to the full compensation of positive charges of CS by the negative charges of GA, which in turn produced uncharged nanoparticles, thus prone to aggregate. Higher turbidity values were obtained when the CS starting solution had a higher concentration (3.0 mg/mL vs. 0.60 mg/mL). This might be due to the higher ionic strength, which improved the interaction of CS and GA, leading to the obtention of a higher number of nanoparticles. There was no significant difference between the process yields of the two studied CS initial concentrations. Dynamic light scattering measurements showed that there was not a significant variation of the hydrodynamic diameter of the nanoparticles, as the number of negatives charges increased. Indeed, the nanoparticles were found to possess hydrodynamic diameters between 400 and 600 nm. Zeta potential measurements of the nanoparticles' suspensions were performed as well, showing that the zeta potential of the nanoparticles did not vary significantly as a function of the number of negative charges added to the medium. The ZP ranged between 30 and 55 mV. Positive ZP values were obtained, up until aggregation occurred at CS:GA charge ratios around 1:1, due to the number of positive charges in the medium being always higher than that of negative charges, so free non-neutralized positive charges were always available at the surface of the nanoparticles, stabilizing them. Regarding the lack of variation on their hydrodynamic diameter with the CS:GA charge ratio, it can be speculated that, due to GA being relatively poorly charged, GA molecules possess large non-charged segments, which are included in the cores of the nanoparticles. Hence, the size reduction of the nanoparticles due to the consumption of superficial positive charges and consequent collapse of the so-formed hydrophobic segments are rendered inapparent.

Transmission electron microscopy and atomic force microscopy imaging provided further insight on the morphology of CS:GA nanoparticles. TEM indicated that the nanoparticles had an average spherical shape, with a considerable degree of polydispersion (confirming DLS previous data), although their sizes were lower than those indicated by DLS, because of the typical shrinking phenomenon in dry environments. Atomic force microscopy imaging showed the relatively smooth surface of the nanoparticles, confirmed their size polydispersion, and revealed the existence of some vesicular structures, as well as particulate complexes. The presence of vesicular structures might be due to the lack of charge neutralization of the positive charges of CS by the negative charges of GA, while their relatively higher abundance at a CS initial concentration of 0.60 mg/mL, when compared to 3.0 mg/mL, might be attributable to the lower overall biopolymer concentration in the first case, which renders the molecules less flexible and thus less favorable for the formation of particulate complexes.

Abbreviations Index

AFM: Atomic force microscopy

ALG: Alginic acid

Aβ: Amyloid-β

BBB: Blood-brain barrier

BLG: β-lactoglobulin

BSA: Bovine serum albumin

CLSM: Confocal laser scanning microscopy

CNS: Central nervous system

CS: Chitosan

DLS: Dynamic light scattering

DS: Dextran sulfate

FITC: Fluorescein isothiocyanate

GA: Gum Arabic

GM: Phosphorylated glucomannan

iAβ5-FITC: FITC-labeled iAβ5 peptide

LbL: Layer-by-layer technique

MTS: Multicellular tumour spheroids

PAH: Poly(allylamine hydrochloride)

PBS: Phosphate buffered saline

PEC: Polyelectrolyte complexation

PEM: Polyelectrolyte multilayer

PGA: Poly-γ-glutamic acid

PLG: Poly(L-glutamic acid)

PLL: Poly(L-lysine)

PMD: Protein misfolding disorders

PS: Polystyrene

PSS: Poly(sodium 4-styrene sulfonate)

TEM: Transmission electron microscopy

TFA: Trifluoroacetic acid

THF: Tetrahydrofuran

TPP: Pentasodium tripolyphosphate

ZP: Zeta potential

References

ADESSI, C.; SOTO, C. - Beta-Sheet Breaker Strategy for the Treatment of Alzheimer's Disease. **Drug Development Research**. 56:(2002). p. 184-193.

AGNIHOTRI, S. A.; MALLIKARJUNA, N. N.; AMINABHAVI, T. M. - Recent advances on chitosan-based micro- and nanoparticles in drug delivery. **Journal of Controlled Release**. 100:(2004). p. 5-28.

AI, H.; PINK, J. J.; SHUAI, X.; BOOTHMAN, D. A.; GAO, J. - Interactions between self-assembled polyelectrolyte shells and tumour cells. **J Biomed Mater Res**. 73A:(2005). p. 303-312.

AKTAS, Y.; ANDRIEUX, K.; ALONSO, M. J.; CALVO, P.; GURSOY, R. N.; COUVREUR, P.; CAPAN, Y. - Preparation and in vitro evaluation of chitosan nanoparticles containing a caspase inhibitor. **International Journal of Pharmaceutics**. 298:(2005). p. 378-383.

ALONSO-SANDE, M.; CUÑA, M.; REMUÑÁN-LÓPEZ, C.; TEIJEIRO-OSORIO, D.; L. ALONSO-LEBRERO, J.; ALONSO, M. J. - Formation of New Glucomannan-Chitosan Nanoparticles and Study of Their Ability To Associate and Deliver Proteins. **Macromolecules**. 39:12 (2006). p. 4152-4158.

ALONSO, M. J. - Nanomedicines for overcoming biological barriers. **Biomedicine & Pharmacotherapy**. 58:(2004). p. 168-172.

AMER, D. A. M.; IRVINE, G. B.; EL-AGNAF, O. M. A. - Inhibitors of α-synuclein oligomerization and toxicity: a future therapeutic strategy for Parkinson's disease and related disorders. **Experimental Brain Research**. 173:2 (2006). p. 223-233.

AN, Z. H.; KAVANOOR, K; CHOY M. L.; KAUFMAN, L. J. - Polyelectrolyte microcapsule interactions with cells in two- and three-dimensional culture. **Colloids and Surfaces B: Biointerfaces**. 70:1 (2009). p. 114-123.

ANTIPOV, A. A.; SUKHORUKOV, G. B.; LEPORATTI, S.; RADTCHENKO, I. L.; DONATH, E.; MÖHWALD, H. - Polyelectrolyte multilayer capsule permeability control. **Colloids and Surfaces a-Physicochemical and Engineering Aspects**. 198:(2002). p. 535-541.

ARIGA, K.; HILL, J. P.; JI, Q. - Layer-by-layer assembly as a versatile bottom-up nanofabrication technique for exploratory research and realistic application. **Physical Chemistry Chemical Physics**. 9:(2007). p. 2319-2340.

BODNAR, M.; HARTMANN, J. F.; BORBELY, J. - Preparation and characterization of chitosan-based nanoparticles. **Biomacromolecules**. 6:(2005). p. 2521-2527.

CALABRIA, A. R.; SHUSTA, E. V. - Blood-brain barrier genomics and proteomics: elucidating phenotype, identifying disease targets and enabling drug delivery. **Drug Discov Today**. 11:(2006). p. 792-799.

CALVO, P.; REMUNAN-LOPEZ, C.; VILA-JATO, J. L.; ALONSO, M. J. - Novel Hydrophilic Chitosan-Polyethylene Oxide Nanoparticles as Protein Carriers. **Journal of Applied Polymer Science**. 63:(1997). p. 125-132.

CARUSO, F. - *Nanoscale particle modification via sequential electrostatic assembly*. Wiley-VCH Verlag GmbH & Co. KGaA: 2004.

CARUSO, F.; NIIKURA, K.; FURLONG, D. N. AND OKAHATA, Y. - 2. Assembly of Alternating Polyelectrolyte and Protein Multilayer Films for Immunosensing. **Langmuir**. 13:13 (1997). p. 3427-3433.

CHEN, Y.; MOHANRAJ, V. J.; WANG, F.; BENSON, H. A. E. - Designing Chitosan-Dextran Sulfate Nanoparticles Using Charge Ratios. **AAPS PharmSciTech**. 8:4 (2007). p. E1-E9.

COUVREUR, P.; VAUTHIER, C. - Nanotechnology: Intelligent Design to Treat Complex Disease. **Pharmaceutical Research**. 23:7 (2006). p. 1417-1450.

CUI, Z. R.; MUMPER, R. J. - Chitosan-based nanoparticles for topical genetic immunization. **Journal of Controlled Release**. 75:(2001). p. 409-419.

DAI, Z.; YIN, J.; YAN, S.; CAO, T.; MA, J.; CHEN, X. - Polyelectrolyte complexes based on chitosan and poly(L-glutamic acid). **Polymer International**. 56:(2007). p. 1122–1127.

DE CAMPOS, A. M.; DIEBOLD, Y.; CARVALHO, E. L. S.; SÁNCHEZ, A.; ALONSO, M. J. - Chitosan nanoparticles as new ocular drug delivery systems: *in vitro* stability, *in vivo* fate, and cellular toxicity. **Pharmaceutical Research**. 21:5 (2004). p. 803-810.

DE SALAMANCA, A. E.; DIEBOLD, Y.; CALONGE, M.; GARCÍA-VAZQUEZ, C.; CALLEJO, S.; VILA, A.; ALONSO, M. J. - Chitosan Nanoparticles as a Potential Drug Delivery System for the Ocular Surface: Toxicity, Uptake Mechanism and In Vivo Tolerance. **Invest. Ophthalmol. Vis. Sci.** 47:4 (2006). p. 1416-1425.

DE KOKER, S.; DE GEEST, B. G.; CUVELIER, C.; FERDINANDE, L.; DECKERS, W.; HENNINK, W. E.; DE SMEDT, S.; MERTENS, N. - In vivo Cellular Uptake, Degradation, and Biocompatibility of Polyelectrolyte Microcapsules. **Advanced Functional Materials**. 17:18 (2007). p. 3754-3763.

DECHER, G. - Fuzzy nanoassemblies: toward layered polymeric multicomposites. **Science**. 277:(1997). p. 123.

DEGEN, P. P.; SHUKLA, A.; BOETCHER, U.; REHAGE, H. - Self-assembled ultra-thin coatings of octadecyltrichlorosilane (OTS) formed at the surface of iron oxide nanoparticles. **Colloid & polymer science**. 286:2 (2008). p. 159-168.

DONATH, E.; SUKHORUKOV, G. B.; CARUSO, F.; DAVIS, S. A.; MÖHWALD, H. - Novel hollow polymer shells by colloid-templated assembly of polyelectrolytes. **Angewandte Chemie-International Edition**. 37:16 (1998). p. 2202-2205.

ESPINOZA-ANDREWS, H.; BÁEZ-GONZÁLEZ, J. G.; CRUZ-SOSA, F.; VERNON-CARTER, E. J. - Gum Arabic-Chitosan Complex Coacervation. **Biomacromolecules**. 8:4 (2007). p. 1313-1318.

ESTRADA, L. D.; SOTO, C. - Inhibition of Protein Misfolding and Aggregation by Small Rationally-Designed Peptides. **Current Pharmaceutical Design**. 12:(2006). p. 2557-2567.

GLINEL, K.; SUKHORUKOV, G.B.; MÖHWALD, H.; KHRENOV, V.; TAUER, K. - Thermosensitive Hollow Capsules Based on Thermoresponsive Polyelectrolytes. **Macromolecular Chemistry and Physics**. 204:14 (2003). p. 1784-1790.

HAJDU, I.; BODNÁR, M.; FILIPCSEI, G.; HARTMANN, J. F.; DARÓCZI, L; ZRÍNYI, M.; BORBÉLY, J. - Nanoparticles prepared by self-assembly of Chitosan and poly-γ-glutamic acid. **Colloid Polym Sci**. 286:3 (2008). p. 343-350.

HAYNIE, D. T.; ZHANG, L.; RUDRA, J. S.; ZHAO, W.; ZHONG, Y.; PALATH, N. - Polypeptide Multilayer Films. **Biomacromolecules**. 6:6 (2005). p. 2895-2913.

HEJAZI, R.; AMIJI, M. - Chitosan-based gastrointestinal delivery systems. **Journal of Controlled Release**. 89:(2003). p. 151-165.

HUCKEL, E. - **Phyzik Z**. 25:204 (1924). p.

IBARZ, G.; DÄHNE, L.; DONATH, E.; MÖHWALD, H. - Smart Micro- and Nanocontainers for Storage, Transport, and Release. **Advanced Materials**. 13:17 (2001). p. 1324-1327.

ILLUM, L. - Chitosan and Its Use as a Pharmaceutical Excipient. **Pharmaceutical Research**. 15:9 (1998). p. 1326-1331.

JAIN, D.; BANERJEE, R. - Comparison of ciprofloxacin hydrochloride-loaded protein, lipid and chitosan nanoparticles for drug delivery. **J Biomed Mater Res**. 86B:(2008). p. 105-112.

JEONG, J. H.; KIM, S. W.; PARK, T. G. - Molecular design of functional polymers for gene therapy. **Progress in Polymer Science**. 32:11 (2007). p. 1239-1274.

JESSEL, N.; ATALAR, F.; LAVALLE, P.; MUTTERER, J.; DECHER, G.; SCHAAF, P.; VOEGEL, J.-C.; OGIER, J. - Bioactive Coatings Based on a Polyelectrolyte Multilayer Architecture Functionalized by Embedded Proteins. **Advanced Materials**. 15:9 (2003). p. 692-695.

JOHNSTON, A. P. R.; CORTEZ, C.; ANGELATOS, A. S.; CARUSO, F. - Layer-by-layer engineered capsules and their applications. **Current Opinion in Colloid and Interface Science**. 11:(2006). p. 203-209.

JOURDAINNE, L.; ARNTZ, Y.; SENGER, B.; DEBRY, C.; VOEGEL, J.-C.; SCHAAF, P.; LAVALLE, P. - Multiple Strata of Exponentially Growing Polyelectrolyte Multilayer Films. **Macromolecules**. 40:2 (2007). p. 316-321.

JUNG, J. E.; MOON, J. Y.; GHIL, S. H.; YOO, B. S. - 2,3,7,8-Tetrachlorodibenzo-p-dioxin (TCDD) inhibits neurite outgrowth in differentiating human SH-SY5Y neuroblastoma cells. **Toxicology Letters**. 188:2 (2009). p. 153-156.

JUNLI, Y.; YANTAO, H.; CHUNBO, W.; WENGONG, Y. - Cytoprotective effect of polypeptide from *Chlamys farreri* on neuroblastoma (SH-SY5Y) cells following H_2O_2 exposure involves scavenging ROS and inhibition JNK phosphorylation. **Journal of Neurochemistry**. 111:2 (2009). p. 441-451.

KOKKONI, N.; STOTT, K.; AMIJEE, H.; MASON, J. M.; DOIG, A. J. - N-Methylated Peptide Inhibitors of β-Amyloid Aggregation and Toxicity. Optimization of the Inhibitor Structure. **Biochemistry**. 45:32 (2006). p. 9906-9918.

LADAM, G.; SCHAAF, P.; CUISINIER, F. J. G.; DECHER, G.; VOEGEL, J.-C. - Protein Adsorption onto Auto-Assembled Polyelectrolyte Films. **Langmuir**. 17:3 (2001). p. 878-882.

LAVALLE, P.; GERGELY, C.; CUISINIER, F. J. G.; DECHER, G.; SCHAAF, P.; VOEGEL, J. C.; PICART, C. - Comparison of the Structure of Polyelectrolyte Multilayer Films Exhibiting a Linear and an Exponential Growth Regime: An in Situ Atomic Force Microscopy Study. **Macromolecules**. 35:11 (2002). p. 4458-4465.

LAVALLE, P.; VIVET, V.; JESSEL, N.; DECHER, G.; VOEGEL, J.-C.; MESINI, P. J.; SCHAAF, P. - Direct Evidence for Vertical Diffusion and Exchange Processes of Polyanions and Polycations in Polyelectrolyte Multilayer Films. **Macromolecules**. 37:3 (2004). p. 1159-1162.

LEE, J. W.; PARK, J. H.; ROBINSON, J. R. - Bioadhesive-based dosage forms: the next generation. **J. Pharm. Sci.** 89:(2000). p. 850-866.

LI, Y.-P.; PEI, Y.-Y.; ZHANG, X.Y.; GU, Z.-H.; ZHOU, Z.-H.; YUAN, W.-F.; ZHOU, J.-J.; ZHU, J.-H.; GAO, X.-J. - PEGylated PLGA nanoparticles as protein carriers: synthesis, preparation and biodistribution in rats. **Journal of Controlled Release**. 71:(2001). p. 203-211.

LIU, Z.; JIAO, Y.; WANG, Y.; ZHOU, C.; ZHANG, Z. - Polysaccharides-based nanoparticles as drug delivery systems. **Advanced Drug Delivery Reviews**. 60:(2008). p. 1650-1662.

LU, B.; XIONG, S.-B.; YANG, H.; YIN, X.-D.; ZHAO, R.-B. - Mitoxantrone-loaded BSA nanospheres and chitosan nanospheres for local injection against breast cancer and its lymph node metastases - I: formulation and in vitro characterization. **International Journal of Pharmaceutics**. 307:(2006). p. 168-174.

MCNAMEE, B. F.; O'RIORDAN, E. D.; O'SULLIVAN, M. - Emulsification and Microencapsulation Properties of Gum Arabic. **J. Agric. Food Chem.** 46:11 (1998). p. 4551-4555.

MINTZER, M. A.; SIMANEK, E. E. - Nonviral Vectors for Gene Delivery. **Chemical Reviews**. 109:2 (2009). p. 259-302.

MORILLE, M.; PASSIRANI, C.; VONARBOURG, A.; CLAVREUL, A.; BENOIT, J.-P. - Progress in developing cationic vectors for non-viral systemic gene therapy against cancer. **Biomaterials**. 29:24-25 (2008). p. 3477-3496.

PAN, Y.; LI, Y.-j.; ZHAO, H.-y.; ZHENG, J.-m.; XU, H.; WEI, G.; HAO, J.-s.; CUI, F.d. - Bioadhesive polysaccharide in protein delivery system: chitosan nanoparticles improve the intestinal absorption of insulin in vivo. **International Journal of Pharmaceutics**. 249:(2002). p. 139-147.

PARTRIDGE, W. M. - *Introduction to the Blood-Brain Barrier: Methodology, Biology and Pathology.* Cambridge: Cambridge University Press, 1998.

PRADIER, C. M.; HUMBLOT, V.; STIEVANO, L.; MÉTHIVIER, C.; LAMBERT, J. F. - Salt Concentration and pH-Dependent Adsorption of Two Polypeptides on Planar and Divided Alumina Surfaces. In Situ IR Investigations. **Langmuir**. 23:5 (2007). p. 2463-2471.

PREGO, C.; FABRE, M.; TORRES, D.; ALONSO, M. J. - Efficacy and Mechanism of Action of Chitosan Nanocapsules for Oral Peptide Delivery. **Pharmaceutical Research**. 23:3 (2006). p. 549-556.

REIS, C. P.; NEUFELD, R. J.; RIBEIRO, A. J.; VEIGA, F. - Nanoencapsulation I: Methods for preparation of drug-loaded polymeric nanoparticles. **Nanomedicine: Nanotechnology, Biology, and Medicine**. 2:(2006a). p. 8-21.

REIS, C. P.; NEUFELD, R. J.; RIBEIRO, A. J.; VEIGA, F. - Nanoencapsulation II. Biomedical applications and current status of peptide and protein nanoparticulate delivery systems. **Nanomedicine: Nanotechnology, Biology, and Medicine**. 2:(2006b). p. 53-65.

RIBEIRO, T.; BALEIZÃO, C.; FARINHA, J. P. S. - Synthesis and Characterization of Perylenediimide Labeled Core-Shell Hybrid Silica-Polymer Nanoparticles. **The Journal of Physical Chemistry C**. 113:42 (2009). p. 18082-18090.

RICHARD, A.; MARGARITIS, A. - Poly(glutamic Acid) for Biomedical Applications. **Critical Reviews in Biotechnology**. 21:4 (2001). p. 219-232.

SANCHEZ, C.; MEKHLOUFI, G.; SCHMITT, C.; RENARD, D.; ROBERT, P.; LEHR, C.-M.; LAMPRECHT, A.; HARDY, J. - Self-Assembly of β-lactoglobulin and Acacia Gum in Aqueous Solvent: Structure and Phase-Ordering Kinetics. **Langmuir**. 18:26 (2002). p. 10323-10333.

SARMENTO, B.; MARTINS, S.; RIBEIRO, A.; VEIGA, F.; NEUFELD, R.; FERREIRA, D. - Development and comparison of different nanoparticulate polyelectrolyte complexes as insulin carriers. **International Journal of Peptide Research and Therapeutics**. 12:2 (2006). p. 131-138.

SCHATZ, C.; DOMARD, A.; VITON, C.; PICHOT, C.; DELAIR, T. - Versatile and Efficient Formation of Colloids of Biopolymer-Based Polyelectrolyte Complexes. **Biomacromolecules**. 5:5 (2004a). p. 1882-1892.

SCHATZ, C.; LUCAS, J.-M.; VITON, C.; DOMARD, A.; PICHOT, C.; DELAIR, T. - Formation and Properties of Positively Charged Colloids Based on Polyelectrolyte Complexes of Biopolymers. **Langmuir**. 20:18 (2004b). p. 7766-7778.

SCHMITT, C.; SANCHEZ, C.; LAMPRECHT, A.; RENARD, D.; LEHR, C.-M.; DE KRUIF, C. G.; HARDY, J. - Study of β-lactoglobulin/acacia gum complex coacervation by diffusing-wave spectroscopy and confocal scanning laser microscopy. **Colloids and Surfaces B: Biointerfaces**. 20:3 (2001). p. 267-280.

SILVANO, D.; KROL, S.; DIASPRO, A.; CAVALLERI, O.; GLIOZZI, A. - Confocal Laser Scanning Microscopy to Study Formation and Properties of Polyelectrolyte Nanocapsules Derived From CdCO3 Templates. **Microscopy Research and Technique**. 59:6 (2002). p. 536-541.

SINHA, V. R.; KUMRIA, R. - Polysaccharides in colon-specific drug delivery. **International Journal of Pharmaceutics**. 224:(2001). p. 19-38.

SMOLUCHOWSKI, M. V. - **Bull Int Acad Sci**. 184:(1903). p.

SOPPIMATH, K. S.; AMINABHAVI, T. M.; KULKARNI, A. R.; RUDZINSKI, W. E. - Biodegradable polymeric nanoparticles as drug delivery devices. **Journal of Controlled Release**. 70:(2001). p. 1-20.

SOTO, C.; SIGURDSSON, E. M.; MORELLI, L.; KUMAR, R. A.; CASTAÑO, E. M.; FRANGIONE, B. - Inhibition of Alzheimer's amyloidosis by peptides that prevent beta-sheet conformation. **Biochem Biophys Res Commun**. 226:(1996). p. 672-680.

SUKHORUKOV, G.; FERY, A.; MÖHWALD, H. - Intelligent micro- and nanocapsules. **Progress in Polymer Science**. 30:(2005). p. 885-897.

TEIXIDÓ, M.; GIRALT, E. - The role of peptides in blood-brain barrier nanotechnology. **Journal of Peptide Science**. 14:(2008). p. 163-173.

UBERTI, D.; PICCIONI, L.; COLZI, A.; BRAVI, D.; CANONICO, P. L.; MEMO, M. - Pergolide protects SH-SY5Y cells against neurodegeneration induced by H2O2. **European Journal of Pharmacology**. 434:1-2 (2002). p. 17-20.

VAUTHIER, C.; DUBERNET, C.; FATTAL, E.; PINTO-ALPHANDARY, H.; COUVREUR, P. - Poly(alkylcyanoacrylates) as biodegradable materials for biomedical applications. **Advanced Drug Delivery Reviews**. 55:(2003). p. 519-548.

VILA, A.; SÁNCHEZ, A.; JANES, K.; BEHRENS, I.; KISSEL, T.; VILA JATO, J. L.; ALONSO, M. J. - Low molecular weight chitosan nanoparticles as new carriers for nasal vaccine delivery in mice. **European Journal of Pharmaceutics and Biopharmaceutics**. 57:(2004). p. 123-131.

WATTENDORF, U.; KREFT, O., TEXTOR, M., SUKHORUKOV, G. B., AND MERKLE, H. P. - Stable Stealth Function for Hollow Polyelectrolyte Microcapsules through a Poly(ethylene glycol) Grafted Polyelectrolyte Adlayer. **Biomacromolecules**. 9:1 (2008). p. 100-108.

WOLFERT, M. A.; DASH, P. R.; NAZAROVA, O.; OUPICKY, D.; SEYMOUR, L. W.; SMART, S.; STROHALM, J.; ULBRICH, K. - Polyelectrolyte Vectors for Gene Delivery: Influence of Cationic Polymer on Byophysical Properties of Complexes Formed with DNA. **Bioconjugate Chem.** 10:6 (1999). p. 993-1004.

WOOD, J. D.; WETZEL, R.; MARTIN, J. D.; HURLE, M. R. - Prolines and amyloidogenicity in fragments of the Alzheimer's peptide b/A4. **Biochemistry**. 34: (1995). p. 724-730.

XU, R. R. - Progress in nanoparticles characterization: Sizing and zeta potential measurement. **Particuology**. 6:2 (2008). p. 112-115.

XU, Y.; DU, Y. - Effect of molecular structure of chitosan on protein delivery properties of chitosan nanoparticles. **International Journal of Pharmaceutics**. 250:(2003). p. 215-226.

ZHAO, W.; ZHENG, B.; HAYNIE, D. T. - A Molecular Dynamics Study of the Physical Basis of Stability of Polypeptide Multilayer Nanofilms. **Langmuir**. 22:15 (2006). p. 6668-6675.

ZHI, J.; WANG, Y. J.; LUO, G. S. - Adsorption of diuretic furosemide onto chitosan nanoparticles prepared with a water-in-oil nanoemulsion system. **React. Funct. Polym.** 65:(2005). p. 249-257.

ZHI, Z.-L.; HAYNIE, D. T. - Direct Evidence of Controlled Structure Reorganization in a Nanoorganized Polypeptide Multilayer Thin Film. **Macromolecules**. 37:23 (2004). p. 8668-8675.

ZHI, Z. L.; HAYNIE, D. T. - Straightforward and effective protein encapsulation in polypeptide-based artificial cells. **Artificial cells, blood substitutes, and immobilization biotechnology**. 34:2 (2006). p. 189-203.

Websites

http://www.britannica.com/EBchecked/topic-art/183561/110686/Transmission-electron-microscope

http://www.lenntech.com/zeta-potential.htm

http://www.microtrac.com/downloads/2006/Nano(US)Web.pdf

http://www.mobot.org/jwcross/spm/notes.htm

http://www.nbtc.cornell.edu/facilities/downloads/Zetasizer%20chapter%2016.pdf

http://www.uk.plbio.kvl.dk/~als/confocal.htm